

Central Queensland University



Experimental Investigation of the Structural Behaviour of Concrete-Filled FRP Tubes

A Dissertation Submitted by

Huigyeong Kim

for the fulfilment of the degree of

Master of Engineering

August 2015

ABSTRACT

Concrete-filled tubes (CFTs) are structural columns used to support compressive loads. A CFT takes advantage of the lateral confinement of the tube on the concrete core to increase the column strength. Since the development of CFT structures, steel has been the primary tube material. Over the last two decades however, fibre reinforced polymers (FRPs) have been increasingly used as tube materials because of their superior properties such as high specific strength and stiffness, superior corrosion resistance and good durability.

This thesis describes a systematic experimental study of CFT columns with FRP as the tube material. This master's project investigates the performance of FRP tubes of different properties and sizes. For this purpose, 12 CFT specimens with the length over diameter (L/D) ratios of 8 and 12, and diameter over tube thickness (D/t) ratios ranging from 11 to 43 were tested under compressive force with both ends of the columns set as pin joints. The experiments were carried out using a heavy loading machine and the experimental results are analysed in terms of strength and failure modes.

The experimental results showed the significant improvements in column strength due to the confinement of the FRP tubes. It was demonstrated that while both L/D and D/t ratios influence column strength, D/t ratio plays a particularly important role in determining the column strength. The experimental results also showed the changes in failure modes with L/D and D/t ratios.

To compare FRP tubes with plain concrete columns, an equivalent slenderness ratio for the CFT with FRP tube was derived. The equivalent slenderness ratio had good agreement with the D/t ratio of the FRP tube. It was demonstrated that the equivalent slenderness can be used to determine the capacity of the CFT column using its D/t ratio.

CERTIFICATION OF DISSERTATION

I certify that the ideas, experimental work, results, analysis, software and conclusions reported in this dissertation are entirely my own effort, except where otherwise acknowledged. I also certify that the work is original and has not been previously submitted for any other award, except where otherwise acknowledged.

Huigyeong Kim
Candidate

ACKNOWLEDGEMENTS

Completion of this dissertation would not have been possible without genuine support and help from a number of people to whom I wish to express my sincere gratitude.

I would like to acknowledge the advice, guidance and support given by my supervisors Dr. T.G. Suntharavadivel (Kumaran) and Dr. Kai Duan during this research project. Without your support it may not have been possible for me to complete this research project – thank you very much.

Sincere thanks are also due to Paul Boyd and the engineering technical staff Ian Tomlinson, Lindsay Dagan, Travis Frame and Paula Frame for their kind support while I was conducting experiments during this project.

Mr. John Revington helped me with my written English language expression. I am grateful for his time and support.

My thanks go to all the staff and research students of the School of Engineering and Technology who helped me in various ways during my stay at Central Queensland University. I also cannot forget my friends and their families, for their kindness and support during my stay in Rockhampton.

I would like to thank my parents and other family members for their encouragement and support during my studies. Finally, my sincere thanks go to my wife, Sunyoung, for her love, patience and support throughout this study.

TABLE OF CONTENTS

ABSTRACT.....	I
CERTIFICATION OF DISSERTATION.....	II
ACKNOWLEDGEMENTS	III
TABLE OF CONTENTS	IV
LIST OF FIGURES	VII
LIST OF TABLES.....	IX
NOTATIONS.....	X
ABBREVIATIONS.....	XI
CHAPTER 1 INTRODUCTION.....	1
1.1 Background.....	1
1.2 Aims.....	2
1.3 Research Significance.....	2
1.4 Research Limitations	3
1.5 Structure of the Thesis	3
CHAPTER 2 LITERATURE REVIEW.....	5
2.1 Application of FRP in Structural Engineering.....	5
2.2 Theory of Confined Columns	5
2.3 Overview of the Column Jacket (tube)	6
2.3.1 Application of the CFT	6
2.3.2 Material characteristics of CFT.....	6
2.4 Review of Experimental Studies - Steel Confinement.....	7
2.5 Review of Analytical Studies - Steel Confinement.....	11
2.6 Review of Experimental Studies - FRP Confinement.....	15
2.7 Review of Analytical Studies - FRP Confinement	18
2.8 Summary	21
CHAPTER 3 METHODOLOGY.....	23
3.1 Objective of Experimental Program	23
3.2 Design of Test Specimen	23
3.3 Material properties.....	28

3.3.1 Concrete	28
3.3.2 FRP tube.....	29
3.4 Instrumentation	30
3.4.1 Load Measurement.....	30
3.4.2 Strain Measurement	31
3.5 Testing procedure.....	32
3.5.1 Test Set-up	32
3.5.2 Testing of specimens.....	33
3.6 Risk Assessment and H&S Procedure	34
3.7 Summary	34
CHAPTER 4 EXPERIMENTAL RESULTS	36
4.1 Overview of the Results.....	36
4.2 Ultimate Behaviour of FRP Columns	38
4.2.1 Behaviour of the Specimens with 100 mm diameter and 3.5 mm wall thickness.....	38
4.2.2 Behaviour of the Specimens with 100 mm diameter and 8.0 mm wall thickness.....	42
4.2.3 Behaviour of the Specimens with 100 mm diameter and 9.0 mm wall thickness.....	44
4.2.4 Behaviour of the Specimens with 150 mm diameter and 3.5 mm wall thickness.....	46
4.2.5 Behaviour of the Specimens with 150 mm diameter and 8.0 mm wall thickness.....	48
4.2.6 Behaviour of the Specimens with 150 mm diameter and 9.0 mm wall thickness.....	51
4.3 Failure Mode & Equivalent Slenderness Ratio.....	53
4.4 General Observations.....	55
4.4.1 Bonding between FRP & Concrete	55
4.4.2 Permanent deformation in FRP pipe	56
CHAPTER 5 CONCLUSTIONS	57
5.1 Conclusions.....	57
5.1.1 Main Conclusion	57
5.1.2 Specific Conclusions.....	57
5.2 Recommendation for the Future Studies.....	58

REFERENCES.....	59
APPENDIX A EXPERIMENTAL DATA.....	62

LIST OF FIGURES

Figure 1: Comparison of CFT behaviour with respect to shape of the tube (a) circular tube (b) square tubes (c) rectangular tubes	9
Figure 2: Comparison of CFT behaviour with respect to D/t ratio	10
Figure 3: Typical $\phi - \lambda$ relation	12
Figure 4: Bilinear simulation of Hosotani et al.'s test results.....	19
Figure 5: Variation of interfacial shear stress along the length of the colum	20
Figure 6: Groups of specimens according to the diameter of FRP tube	24
Figure 7: FRP tubes with a variety of diameters and wall thicknesses	25
Figure 8: Wrapped FRP tubes	26
Figure 9: Slump test of concrete	28
Figure 10: Compressive strength test.....	29
Figure 11: Uniaxial loading machine.....	31
Figure 12: Strain gauges attached to the FRP tube	31
Figure 13: Measurement system instrument (Signal Express & NI 9219)	32
Figure 14: Set-up the FRP Column.....	33
Figure 15: Filling the gaps with mortar	33
Figure 16: Steel cage.....	34
Figure 17: Steel plate and timber	34
Figure 18: Load-deflection behaviour of specimens with 100 mm diameter and 3.5 mm wall thickness (D100T3A).....	38
Figure 19: Change of texture	39
Figure 20: Strain-deflection behaviour of specimen D100T3A.....	40
Figure 21: Load-deflection behaviour of specimen D100T3B	41
Figure 22: Strain-deflection behaviour of specimen D100T3B.....	41
Figure 23: Load-deflection behaviour of specimens with 100 mm diameter and 8.0 mm wall thickness	42
Figure 24: Strain-deflection behaviour of specimen D100T8A.....	43
Figure 25: Strain-deflection behaviour of specimen D100T8B.....	44

Figure 26: Load-deflection behaviour of specimens with 100 mm diameter and 9.0 mm wall thickness	44
Figure 27: Strain-deflection behaviour of specimen D100T9A.....	45
Figure 28: Strain-deflection behaviour of specimen D100T9B.....	46
Figure 29: Load-deflection behaviour of specimens with 150 mm diameter and 3.5 mm wall thickness	46
Figure 30: Strain-deflection behaviour of specimen D150T3A.....	47
Figure 31: Strain-deflection behaviour of specimen D150T3B.....	48
Figure 32: Load-Deflection behaviour of specimens with 150 mm diameter and 8.0 mm wall thickness	48
Figure 33: Buckling in specimen D150T8A.....	49
Figure 34: Strain-deflection behaviour of specimen D150T8A.....	49
Figure 35: Strain-deflection behaviour of specimen D150T8B.....	50
Figure 36: Load-deflection behaviour of specimens with 150 mm diameter and 9.0 mm wall thickness	51
Figure 37: Strain-deflection behaviour of specimen D150T9A.....	52
Figure 38: Strain-deflection behaviour of specimen D150T9B.....	52
Figure 39: Variation of equivalent slenderness ratio with D/t ratio.....	55
Figure 40: De-bonding between FRP tube and concrete column	55

LIST OF TABLES

Table 1: Properties of concrete-filled steel tube components	8
Table 2: Factors levels selected for each length of the CFT column	13
Table 3: Details of CFT samples tested for each 1m, 0.7 m and 0.5 m length of the column	14
Table 4: L9 – Orthogonal array adopted and experimental results – for each length of CFT	14
Table 5: Properties of concrete specimens.....	18
Table 6: Details of specimen (as per initial plan)	27
Table 7: Compressive strength of concrete.....	29
Table 8: Properties of FRP tubes	30
Table 9: Specification of HCC200 load cell	31
Table 10: Summary of experimental results	37
Table 11: Variation of ultimate load with slenderness of the column	54
Table 12: Permanent deformation of the specimens	56

NOTATIONS

A_c	Area of concrete
$A_{e,con}$	Equivalent area of concrete
A_{FRP}	Area of FRP tube
A_s	Area of steel
A_{total}	Total Area
D	Diameter
E_c	Modulus of elasticity of concrete
E_{FRP}	Modulus of elasticity of FRP
E_s	Modulus of elasticity of steel
f'_c	Characteristic strength of concrete
f_{cu}	Ultimate compressive strength concrete
f_{co}	Compressive strength of unconfined specimen
$f_{le,FRP}$	Effective tensile stress at failure of FRP sheet
f_y	Ultimate strength of steel
K_{coh}	Cohesive shear stiffness
L	Wall Length
L_e	Effective length
N_u	Ultimate strength of the column
N_{uo}	Sectional strength of the column (with no bending moment)
r	Radius of gyration
t	Wall thickness
α	Steel ratio
λ	Slenderness ratio

ABBREVIATIONS

ACI	American Concrete Institute
CFRP	carbon fibre reinforced polymer
CFT	concrete-filled tube
CQU	Central Queensland University
FEA	finite element analysis
FRP	fibre reinforced polymer
SD	standard deviation

Chapter 1

INTRODUCTION

1.1 Background

Western underground mining has undergone drastic changes in the last century, especially since mechanisation was introduced in the early 1900s, signalling the first improvements in mining system efficiency. The trend continues, with modern improvements in long wall supports seen over the years as the result of developments in construction technologies. Wood cribbing was once the dominant type of roof control in underground mines but has been phased out in recent years due to the structural superiority of materials such as steel and concrete. Roof supports in underground mines have seen extensive development over the last century but the basic concept underlying these is the principle of the column. The column is a fundamental structural member designed to resist axial compression forces from other members and from loads above, and transmit them to members below. Concrete is one of the main materials used to construct columns and the associated technology has seen various improvements and innovations over the last two hundred years. Reinforced concrete which uses reinforcing steel bars or ‘rebars’ was introduced in the mid-19th century and it is still used in concrete column structures to this day because of its proven strength, durability, flexibility in use, overall value and widespread availability. Transverse reinforcement was then considered and the concrete-filled tube (CFT) was developed based upon this continuously reinforced principle. CFT columns have been widely use in buildings and bridges. They work more efficiently than reinforced concrete columns for their specific applications.

The CFT, which is based on the principle of the tube, has become the most dominant standing roof support in Western mines in this day and age but alternatives such as the Cluster Prop, Rocprop, and Omni Prop are being investigated to address its shortcomings (Barczak & Tadolini 2005). With the introduction, in recent years, of fibre reinforced polymer (FRP) confining tubes, there is now more scope for improvement of the tube due to their high strength and durability characteristics as well as their resistance to corrosion and light weight.

This project aims to investigate the mechanical performance of FRP-confined CFTs in order to provide adequate information for further improvements of CFT columns. For this purpose, an experimental research plan has been developed. The experimental investigations were carried out using CFT columns confined by FRP tubes, which were subjected to static axial compression loads.

1.2 Aims

The primary objective of this project is to investigate the structural behaviour of FRP-confined CFT columns under uniaxial compressive load.

To achieve this objective, following specific tasks were chosen:

- Conduct a comprehensive literature review to understand the current state-of-art research finding in the relevant area.
- Study FRP properties and investigate the best option for tube materials. The tube is specifically designed to carry large axial load with minimum bending moment that will ensure high mobility for the concrete.
- Investigate the behaviour of FRP-confined tubes under uniaxial compressive load. Investigate failure mode, load-deflection and maximum capacity with varying slenderness ratios (Diameter (D)/Wall thickness (t) & Length (L)/ Wall thickness (t)).

1.3 Research Significance

CFT columns are the most preferred supporting system in the mining industry. Currently, steel has been used as the tube material. The weight of these tubes is considerable. As FRP has a higher strength-to-weight ratio, the use of FRP as an alternative material can reduce the weight of the supporting system, thereby increasing portability. Research into the use of FRP in structural engineering is still in its early stages and there are no standards for manufacturing FRP structural members. The results from this project will increase the understanding of FRP tubes and encourage further input into the literature to develop an Australian Standard for FRP structural members. Moreover, this research provides an economical alternative for mining companies.

1.4 Research Limitations

Due to time and other limitations, the research scope is limited to uniaxial loading on FRP tubes. Therefore, following items are not considered in this study:

1. Bending moment or eccentric loading – bending moment and eccentric loading are important in designing columns, however in the mobile columns that are used in underground mining the effects of bending moment and eccentricity are not significant.
2. Variations in FRP material properties – the material properties of FRP vary depending on the composites, the orientation of the layers, and other factors. In this study only one kind of FRP is considered due to the time and resource limitation.

1.5 Structure of the Thesis

This thesis is divided into five chapters including this introductory chapter. A brief summary of each chapter is shown below.

Chapter 1, the current chapter, brief outlines the background and significance of the research project. It also explains the objective of the research and the structure of the dissertation.

In **Chapter 2**, a comprehensive literature review related to this study is presented. A brief introduction to the structural application of concrete-filled tubes, different conceptual models and research findings related to the application are summarised in this chapter.

To study the behaviour of concrete-filled FRP tubes, eighteen beams were prepared and tested in the civil engineering laboratory of Central Queensland University. Details of the experimental program methodology are given in **Chapter 3**. Details of test specimens, material properties, instrumentation, and testing procedures are briefly explained in this chapter.

The results obtained from the experimental program are presented in **Chapter 4**. A brief discussion of the behaviour of concrete-filled FRP tubes and the influence of the diameter and wall thickness of the tubes is also presented in Chapter 4.

Finally, **Chapter 5** presents the general and specific conclusions of this research study followed by recommendations for future research in this area.

Further information on the experimental results, material data and other relevant information is given in appendices.

Some of this research has been published or is being published in journals and peer-reviewed conferences. Details are provided below:

1. **H. Kim**, T.G. Suntharavadivel and K. Duan (2015), Effectiveness of Concrete-filled FRP Tubes Under Axial Loading, 8th International Structural Engineering and Construction Conference (ISEC8), Sydney, Australia (*accepted*).
2. **H. Kim**, T.G. Suntharavadivel and K. Duan (2014), Experimental Study of Concrete-filled FRP Tubes under Axial Loading, 5th International Conference on Sustainable Built Environment (ICSBE2014), Kandy, Sri Lanka.
3. **H. Kim**, T.G. Suntharavadivel and K. Duan (2013), Investigating the Structural Behaviour of Concrete-filled 'CAN' Under Axial Loading, 26th Biennial Conference of Concrete Institute of Australia (Concrete 2013), Gold Coast, Australia.
4. **H. Kim**, T.G. Suntharavadivel and K. Duan (2013), Overview of Application of Concrete-filled Tube (CFT) in Structural Engineering, 8th Structural Integrity and Fracture Conference, Melbourne, Australia.
5. J. Bobadilla, **H. Kim**, T.G. Suntharavadivel and K. Duan (2013), Behaviour of the Concrete-filled FRP 'Can' Under Axial Loading, 7th International Structural Engineering and Construction Conference (ISEC7), Honolulu, USA.

Chapter 2

LITERATURE REVIEW

2.1 Application of FRP in Structural Engineering

FRP composites were first used in the defence industry, and since then their use has been widely extended. Apart from their military applications, they have been used in fiberglass pipes, and in equipment in the chemical processing and manufacturing industries. Furthermore, since FRP composite products were first used to reinforce concrete structures in the mid-1950s, they have been utilised as construction materials for several decades. In architectural applications, they have been used in semi-permanent structures and in the restoration of historic buildings and for structural applications. In Europe and Asia, many FRP composite products were used during the late 1970s and early 1980s. In Germany, for instance, the world's first highway bridge using composite reinforced tendons was built in 1986. In China, the first all-composite bridge deck was built. The first all-composite pedestrian bridge was completed in 1992 in Aberfeldy, Scotland. In the U.S., the first FRP reinforced concrete bridge deck was constructed in 1996 at McKinley Ville, WV followed by the first all-composite vehicular bridge deck in Russell, KS. Numerous composite pedestrian bridges have been mounted in U.S. state and national parks in remote locations not accessible to heavy construction equipment. They have also been used for spanning roadways and railways (ACMA 2004).

2.2 Theory of Confined Columns

It is well known that concrete members subjected to compression loads under confinement exhibit ductile behaviour with considerable plastic hardening, unlike unconfined concrete which shows quasi-brittle or strain-softening behaviour. This improved behaviour has led to the use of fibre-reinforced plastic (FRP) wraps as confinement for concrete columns. These wraps are comparatively lightweight, they are not susceptible to corrosion, and they have high chemical resistance to environmental effects. Concrete columns confined with FRP

wraps are said to be under passive confinement. When loaded elastically with moderate loads, the confinement has little effect on the force–displacement behaviour of the column, since in the elastic zone concrete undergoes little lateral expansion under the relatively small loads. The FRP casings, which can be analysed as thin hollow cylinders under internal pressure, therefore experience small hoop expansions and hence insignificant strains in the radial direction. On plastification, small stress changes cause comparatively larger radial expansions of the concrete column, resulting in higher internal pressures on the FRP. This in turn mobilises higher confining stresses. These confining stresses limit the expansion and growth of tensile cracks in the concrete and result in higher failure loads. These behaviours, and the explanation thereof, are well known. FRP wraps made of high-stiffness FRP materials, or with a large number of FRP layers, result in higher confining pressures and hence higher failure loads. This has been proven both by experimentally as well as numerically (Dandapat, Deb & Bhattacharyya 2011).

2.3 Overview of the Column Jacket (Tube)

2.3.1 Application of the CFT

At the primary point of application, the CFT columns have large diameters, ranging from 2.3 to 3.3m for high buildings. These columns have target strengths of 96MPa and cylinder strengths of 130 MPa with D/t ratios ranging from 180 to 250 and L/D ratios ranging from 2 to 14. Smaller CFTs have also been used in low- to mid-rise construction projects. Circular CFTs have been used in braced frames, and smaller parts have been used in moment-resisting frames. Compared to extremely large CFTs, the steel tube dimensions are in a more practical range of 0.36-0.76 m for use in low- to mid-rise buildings. D/t ratios for the smaller diameter CFTs ranged from 26 to 48 and L/D ratios ranged from 5 to 9. These smaller CFTs are used for the most common applications in current building construction (Schneider 1998).

2.3.2 Material Characteristics of CFT

FRP provides an interesting type of reinforcement, featuring linear elastic behaviour up to failure, and exerting an increasing confining pressure on the concrete core, leading to enhanced strength and ductility of the concrete when loaded axially (Antonio & Nick 1994; Buyukozturk & Hearing 1998; Mirmiran & Shahawy 1997; Oral, Oguz & Erdem 2003; Samaan, Mirmiran & Shahawy 1998).

Compared to solutions based on concrete-filled steel tubes, FRP reinforcement has a competitive advantage in terms of transport to building site (low density) and high corrosion resistance in harsh environments (ACI Committee 440 1996).

FRPs are currently chosen for some purposes: when local strengthening is needed without modification of the elastic stiffness of structural members, when minimisation of the mass of the building is required, when corrosion-resistance strengthening is required, and when ease of application and reduction of the non-operational period of structure during interventions are preferred (Rousakis & Karabinis 2012).

CFTs are generally regarded as having advantageous features for use in regions at high seismic risk. However, if the load is offered to the concrete core and the steel tube simultaneously, the steel tube expands more than the concrete core, because Poisson's ratio is higher for the steel part (Schneider 1998).

2.4 Review of Experimental Studies – Steel Confinement

Gardner and Jacobson (1967) carried out experiments with CFT columns having D/t ratios ranging from 30 to 40. Their results indicated that when the CFTs reached their ultimate loads, the steel jacket reached failure but the concrete did not. The strain on the steel tube increased without local buckling and the steel tube was provided stabilisation by the concrete.

Tomii, Yoshimura and Morishita (1977) conducted an experiment with almost 270 CFT specimens having circular, square and octagonal cross-sections. They had D/t ratios from 19 to 75 and L/D ratios from 2 to 9. The columns with circular cross-sections and most of the columns octagonal cross-sections showed post-yield behaviour due to the variation in strain hardening of perfectly plastic sections.

Schneider (1998) tested 14 specimens under concentric axial compression. The specimens were three circular, five square, and six of rectangular steel tubes. As shown in Table 1, D/t ratios in this study ranged from 17 to 50 and L/D ratios ranged between 4 and 5.

Table 1: Properties of concrete-filled steel tube components

Shape	Outer nominal diameter (mm)	Actual dimensions (mm)	Actual wall thickness (mm)	<i>D/t</i> ratio	<i>L/D</i> ratio
C1	140	140.8	3.00	47.0	4.3
C2	140	141.4	6.50	21.7	4.3
C3	140	140	6.68	21.0	4.4
S1	127 × 127	127.3 × 127.3	3.15	40.4	4.8
S2	127 × 127	126.9 × 126.9	4.34	29.2	4.8
S3	127 × 127	126.9 × 127.0	4.55	27.9	4.8
S4	127 × 127	125.3 × 126.5	5.67	22.3	4.8
S5	127 × 127	126.8 × 127.2	7.47	17.0	4.8
R1	76 × 152	76.6 × 152.3	3.00	50.8	4.0
R2	76 × 152	76.5 × 152.8	4.47	34.2	4.0
R3	102 × 152	101.8 × 152.4	4.32	35.3	4.0
R4	102 × 152	102.8 × 152.7	4.57	33.4	4.0
R5	102 × 152	101.3 × 151.4	5.72	26.5	4.0
R6	102 × 152	101.13 × 152.37	7.34	20.8	4.0

Source: Schneider (1998)

This experiment produced results which depend on two kinds of parameters.

1. The test results are presented according to tube shape and Figure 1 shows the behaviour of the circular, square and rectangular steel tubes separately. Because of an underestimation of the storage capacity needed for the test data, the data for specimen C3 beyond a load of 1,850 kN was not recorded. However, the yield strength of the specimen was approximated at 2,010 kN during the test. The maximum load for the specimen was accurately measured at 2,710 kN through the fixed frame. Circular tube shapes generally displayed strain-hardening characteristics long after the CFT reached yield. Square and rectangular tube shapes behaved differently to circular tubes. Depending on the tube wall thickness, those tube shapes presented various post-yield behaviours. Local wall buckling did not take place for any specimen prior to yield of the CFT. Furthermore, higher axial deformations were sustained prior to local wall buckling, for the thicker tubes of each shape type.

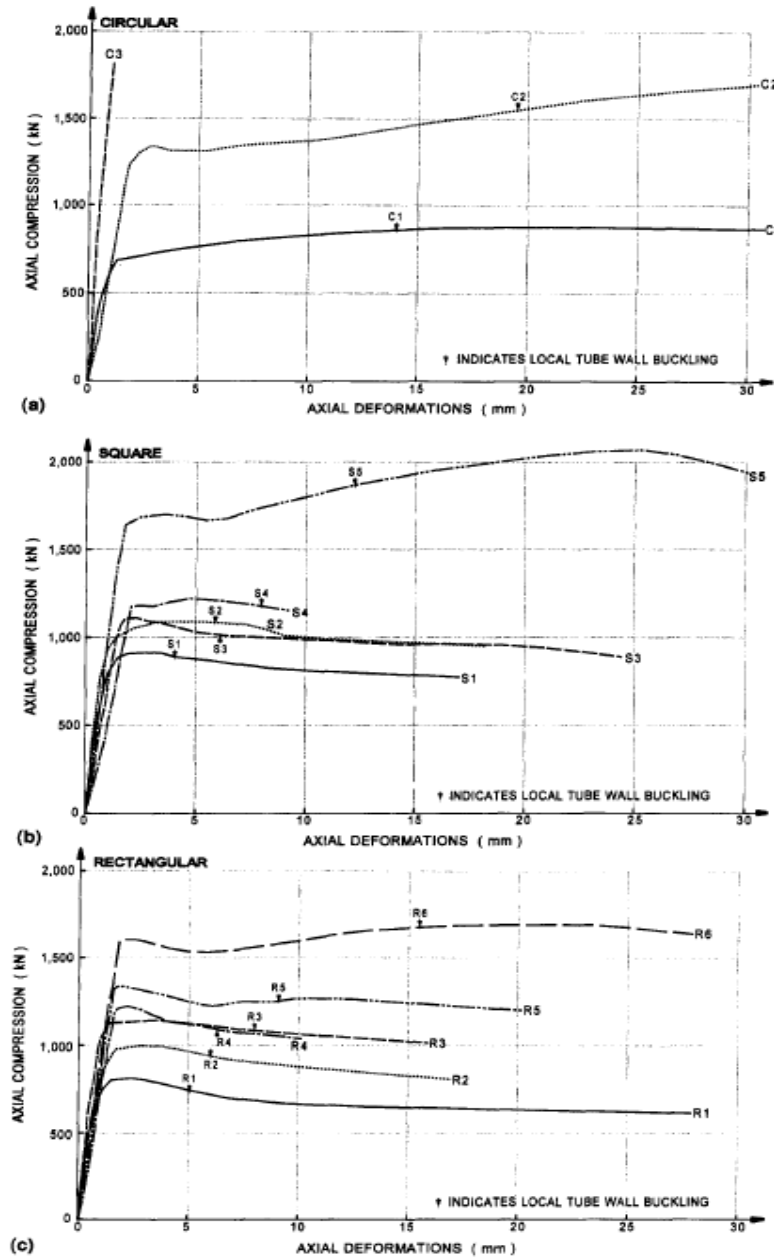


Figure 1: Comparison of CFT behaviour with respect to shape of the tube (a) circular tube (b) square tubes (c) rectangular tubes

Source: Schneider (1998)

2. The D/t ratio became the parameter for arrangement of the test results, as shown in Figure 2. According to d, there was a connection between the D/t ratio and the post-yield behaviour for the square and rectangular tubes. There were three types of post-yield behaviour for noncircular CFT shapes. S5 presented clear signs of strain-hardening behaviour and S5, S4, R5 and R6 exhibited a significant transition from strain-hardening to mildly elastic-plastic. Lastly, the post-yield behaviour for the remaining noncircular CFT shapes was clearly strain-softening. In contrast, C1 was obviously stain-hardening even if the D/t ratio was larger than other specimens.

Local buckling for all CFTs with strain-softening post-yield behaviour took place at an axial ductility of between 2 and 6. For the square and rectangular strain-hardening specimens, local buckling took place at between 6 and 8, while wall buckling did not take place for the circular tube until 10 or more.

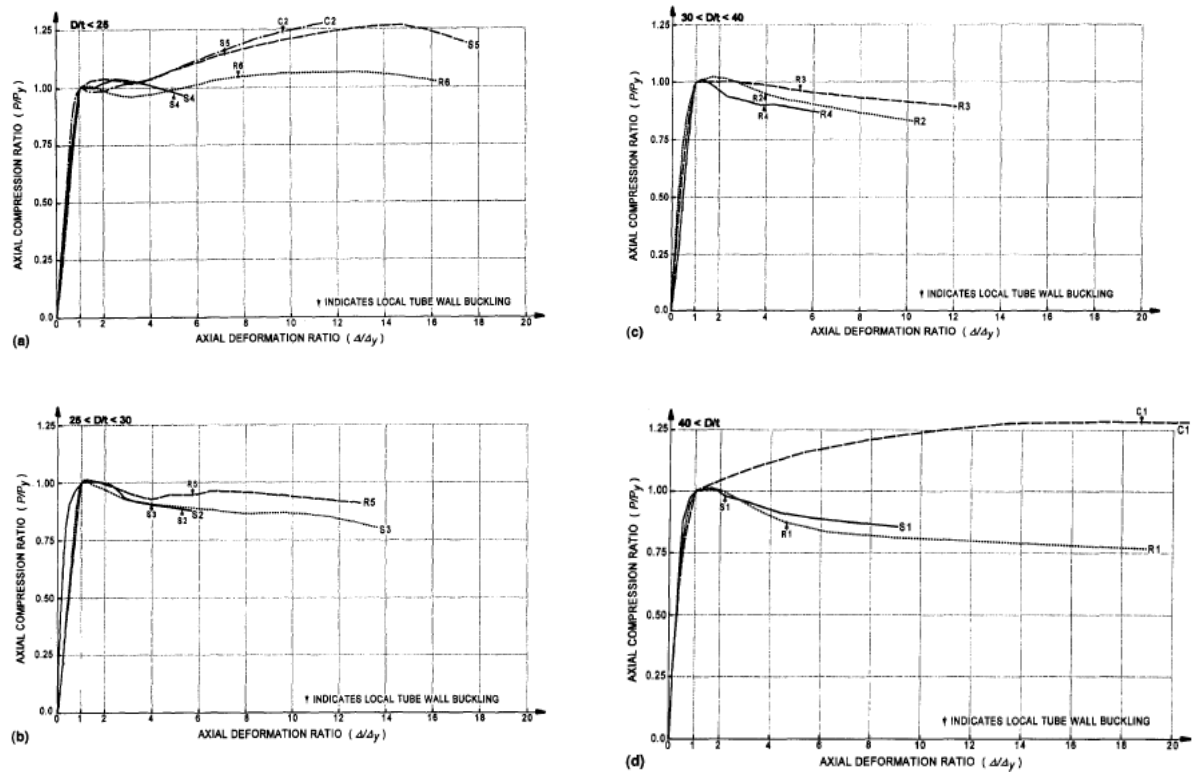


Figure 2: Comparison of CFT behaviour with respect to D/t ratio

(a) $D/t < 25$ (b) $25 < D/t < 30$ (c) $30 < D/t < 40$ (d) $40 < D/t$

Source: Schneider (1998)

In this experiment, it was shown that circular steel tubes offer much more post-yield axial ductility than square or rectangular tubes. All circular tubes were categorised as strain-hardening. On the other hand, the square and rectangular tube walls, in general, did not offer substantial concrete confinement beyond the yield load of the composite column.

O'Shea and Bridge (1998) carried out an experimental analysis with circular steel tube specimens which were filled with medium (50 MPa) and high strength (80 MPa) concrete. They had various D/t ratios from 59 to 221 and L/D ratios ranging from approximately 3 to 4. Confinement of the medium strength mix occurred in tubes with D/t ratios ranging from 59 to 221 while the high strength concrete mix resulted in confinement only at ratios lower than 125. There are two types of failure models for steel tubes. In the first type the bond between the steel tube and the concrete is maintained the axial strength of the steel tube. In the second

type the bond is not maintained and there is local buckling of the steel tube. While even thin-walled steel tubes were found to improve the ultimate strength and ductility of the medium strength concrete (50 MPa) under uniaxial loading and at small eccentricities, confinement of the high strength concrete (80 MPa) only occurred for the thicker steel tubes under uniaxial loading and at small eccentricities.

Huang et al. (2002) carried out an analytical experiment to investigate the behaviour of CFT steel columns under axial loading. Seventeen specimens were prepared with D/t ratios ranging from 40 to 150 and two types of cross-section: circular and square. As a result, it was found that the CFT columns with circular cross-sections performed better than square columns regardless of the D/t ratio, and a smaller D/t ratio produced better results.

Sundarraja and Prabhu (2011) investigated the strengthening of CFST members under compression using CFRP composites. Of the 21 specimen columns used in this experiment, 18 were externally reinforced by CFRP strips having a constant width of 50 mm with spacing values of 20 mm and 30 mm, while the remaining three columns were not. One of the main materials in this study was MBrace 240 fabricated by BASF India Inc., unidirectional carbon fibre. It had a modulus of elasticity of 240 kN/mm² and a tensile strength of 3800 N/mm². The thickness of the fibre was 0.234 mm. Another main material was square hollow steel tubing conforming to IS 4923-1977 and IS 1161-1998 with a dimension of 91.5×91.5 mm². It had a thickness of 3.6 mm and a height of 600 mm.

2.5 Review of Analytical Studies – Steel Confinement

Hsuan-Teh et al. (2003) analysed steel CFT columns numerically under axial compressive loading using the nonlinear finite element program ABAQUS. D/t ratios ranging from 17 to 150 were analysed for circular and square tubes with and without stiffening ties. They found that decreases in D/t ratio provided increases in lateral confinement strength. On the other hand, increases in D/t ratios resulted in more significant lateral deformation in the radial directions, especially in the middle of the CFT columns. For circular columns, the concrete and steel were in full contact, resulting in no local buckling of the tube at axial strains close to 0.025 owing to a uniformly applied confining pressure in all radial directions, while for square columns, the lateral confining pressure is not uniformly applied to the concrete surface, resulting in local buckling of the tube because there is not full contact between the concrete and the steel.

There are three kinds of failure of CFST columns under axial compression according to slenderness ratios, which are intensity failure, elastic-plastic instability failure and elastic instability failure (Han 2007). According to Han (2007), the ratio of stability φ and slenderness ratio λ are defined as follows:

$$\varphi = \frac{N_u}{N_{uo}} \quad (2.1)$$

Where

N_u = ultimate strength of the composite column and
 N_{uo} = sectional strength of the composite column.

$$\lambda = \frac{L_e}{r} = \frac{4L_e}{D} \quad (2.2)$$

Where

L_e = effective column length
 r = radius of gyration and
 D = outer diameter of the compressive section.

Figure 3 shows that intensity failure, elastic-plastic instability failure and elastic instability failure occur when $\lambda \leq \lambda_0$, $\lambda_0 < \lambda \leq \lambda_p$ and $\lambda > \lambda_p$, respectively.

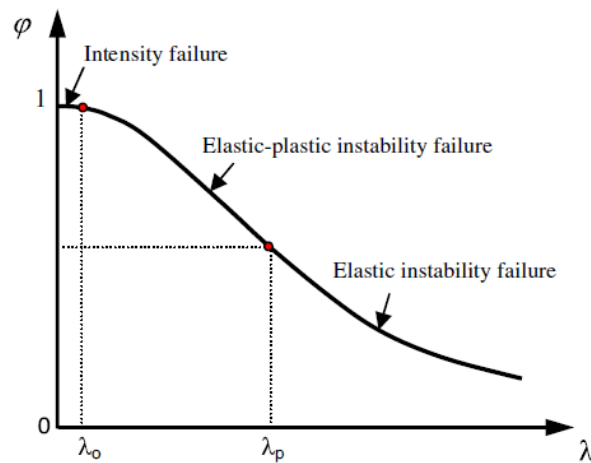


Figure 3: Typical φ - λ relation

Source: Han, 2007

Liang, Q. Q. (2009) used a performance-based analysis (PBA) technique to analyse the effects of D/t ratios, concrete strength, steel yield strength and axial loading on the stiffness, strength and ductility of high-strength CFT columns confined with thin-walled steel tubes. D/t ratios of 40, 70 and 100 were tested and it was found that the axial performance of the specimens decreased as the D/t ratio increased. Increases in this ratio led to reductions in the local buckling strengths of the steel tubes. Once a very high strength concrete was utilised (100 MPa) in association with very slender steel tubes with a D/t ratio of 100, the axial performance index of the section was very low. Reductions in flexural stiffness and strength, curvature ductility and section interaction performance were also noted with an increased D/t ratio.

Choi and Xiao (2010) studied the axial loading behaviour of short CFT columns using results from the experiments of Huang et al. (2002), Tomii, Yoshimura and Morishita (1977) and Schneider (1998). Their research also noted that strain hardening happened for specimens with smaller D/t ratios (less than 50) and lower concrete strength (22–23 MPa) while strain softening (shear resistance is reduced with the continuous development of plastic shear strains) happened for specimens with higher D/t ratios and higher concrete strengths.

Manojkumar, Mattur and Kulkarni (2010) examined the effect of parameters such as: diameter of the steel tube (D), wall thickness of the steel tube (t), strength of in-fill concrete (f_{cu}), and length of the tube (L).

Table 2 shows that they considered three different diameters, wall thickness and grades of concrete. Through using the Taguchi method, this study tried to find an appropriate combination of structural parameters and to conduct the analysis with the minimum number of experiments. They tested 243 circular CFT samples including an L9 orthogonal array as shown in Table 3 and Table 4.

Table 2: Factors levels selected for each length of the CFT column

Levels	Factors		
	Diameter of the steel tube (mm)	Wall thickness of the steel tube (mm)	Strength of in-filled concrete (N/mm ²)
Level-1	44.45	1.25	42.4
Level-2	57.15	1.6	51.7
Level-3	63.5	2	60.7

Source: Manojkumar et al. 2010

Table 3: Details of CFT samples tested for each 1m, 0.7 m and 0.5 m length of the column

Sl. No.	Notation	No. of sample	Notation	No. of sample	Notation	No. of sample
1	$D_1t_1M_{30}$	3	$D_2t_1M_{30}$	3	$D_3t_1M_{30}$	3
2	$D_1t_2M_{30}$	3	$D_2t_2M_{30}$	3	$D_3t_2M_{30}$	3
3	$D_1t_3M_{30}$	3	$D_2t_3M_{30}$	3	$D_3t_3M_{30}$	3
4	$D_1t_1M_{40}$	3	$D_2t_1M_{40}$	3	$D_3t_1M_{40}$	3
5	$D_1t_2M_{40}$	3	$D_2t_2M_{40}$	3	$D_3t_2M_{40}$	3
6	$D_1t_3M_{40}$	3	$D_2t_3M_{40}$	3	$D_3t_3M_{40}$	3
7	$D_1t_1M_{50}$	3	$D_2t_1M_{50}$	3	$D_3t_1M_{50}$	3
8	$D_1t_2M_{50}$	3	$D_2t_2M_{50}$	3	$D_3t_2M_{50}$	3
9	$D_1t_3M_{50}$	3	$D_2t_3M_{50}$	3	$D_3t_3M_{50}$	3
No. of samples	D_1 Series	27	D_2 Series	27	D_3 Series	27

Note: M_{30} = Concrete Mix of characteristic strength of 30 N/mm² with cube strength at 28 days is 42.4 N/mm²
 M_{40} = Concrete Mix of characteristic strength of 40 N/mm² with cube strength at 28 days is 51.7 N/mm²
 M_{50} = Concrete Mix of characteristic strength of 50 N/mm² with cube strength at 28 days is 60.7 N/mm²
Source: Manojkumar et al. 2010

Table 4: L9 – Orthogonal array adopted and experimental results – for each length of CFT

Notation	Ultimate Axial Load P_{ue} (kN)			Axial shortening at ultimate point δ_{ue} (mm)		
	1 m	0.7 m	0.5 m	1 m	0.7 m	0.5 m
$D_1t_1M_{30}$	45.2	82	96.2	4.0	4.7	5.4
$D_1t_2M_{40}$	86.5	117.1	134.1	4.1	5.0	5.2
$D_1t_3M_{50}$	124	145.3	155.6	4.2	5.3	5.4
$D_2t_1M_{40}$	151.6	176.5	187.5	6.0	6.3	5.6
$D_2t_2M_{50}$	181.7	201.5	229	5.4	6.1	5.3
$D_2t_3M_{30}$	144.3	205.8	213.7	8.4	7	7.3
$D_3t_1M_{50}$	181.2	239.1	262.4	4.7	5.8	6.4
$D_3t_2M_{30}$	185.6	226.3	230.5	7.4	7.6	7.8
$D_3t_3M_{40}$	231.3	269	280.5	7.1	7.2	7.4

Source: Manojkumar et al. 2010

From this research, it was found that increases in diameter, wall thickness and concrete strength will increase the ultimate axial load and capacity for 1m, 0.7m and 0.5m lengths of CFTS. Among these parameters, the diameter of the steel tube in particular affected the ultimate axial load capacity and brought about a corresponding axial shortening of all the three lengths of the CFT. The increase of wall thickness helped to delay buckling failure.

Although, there has been a large amount of research work on slender tubular CFST columns, few of the test specimens have had a slenderness ratio bigger than 120. Yu-Feng, Lin-Hai and Xiao-Ling (2012) developed a finite element model to perform mechanism analysis and parametric studies for very slender CFST columns, which have slenderness ratios (λ) bigger than 120. The ABAQUS/Standard module was used to conduct this analysis, and both material and geometric nonlinearities are considered. To describe the constitutive behaviour of steel, an elastic-plastic model was used. A five-stage stress-strain model was applied. The modulus of elasticity and Poisson's ratio of steel are taken as 206 GPa and 0.3, respectively. For concrete, $4730\sqrt{f'_c}$ according to ACI Committee 318 (2008) was taken as the modulus of elasticity and 0.2 as Poisson's ratio. The end plates and core concrete were simulated by an eight-node 4-D solid element, and a four-node conventional shell element was applied for the steel tubes. For the contact between the steel tubes and the inner concrete, hard contact was put to use in the normal direction and the Mohr-Coulomb friction model was utilised in the tangential direction. The frictional coefficient was chosen as 0.6. For the boundary condition, the end plate was presumed to be an elastic rigid block, and the modulus of elasticity and Poisson's ratio of the end plate were given as 1000 GPa and 0.0001, respectively.

As a result of this analysis, firstly, there was a difference between the typical failure models of very slender CFST columns and the reference hollow steel tubular members. The failure mode of very slender circular CFST column is elastic and unstable according to Han (2007). After reaching ultimate strength, local buckling of the steel tube was prevented owing to the core concrete of the CFST column, while the local buckling took place at mid-height level for hollow steel tubular members. It was reported that as the slenderness ratio (λ) increased, ultimate strength decreased while the steel ratio (α) and concrete strength (f_{cu}) increased as strength increased.

2.6 Review of Experimental Studies – FRP Confinement

Bouchelaghem, Bezazi and Scarpa (2011) used two specific composite layups (bidirectional fabrics $(0/90)_2$ and $(+30/-60)_2$). The first provided the highest time to failure, the second showed an increase of up to 70% in strengthening efficiency compared with non-reinforced columns. Six hybrid composite jacket configurations were also investigated. They were: hybrid 1: fabric 1 and mat, hybrid 2: mat and fabric1, hybrid 3: fabric 2 and mat, hybrid 4: mat and fabric 2, hybrid 5: fabric 2 and fabric 1, and hybrid 6: fabric 1 and fabric 2. Mat,

fabric 1 and fabric 2 had surface densities of 300 g/m^2 , 300 g/m^2 and 500 g/m^2 respectively. The results of this work results in the following conclusions: The fibre orientations and the thickness of the wall of the FRP wrapping have a considerable effect on the load-time history, strength, ductility, and damage modes of the composite concrete columns. The composite E-glass fibre/polyester is the most effective material for wrapping concrete columns externally.

The extensive experimental program at the Reinforced Concrete Laboratory of Democritus at the University of Thrace has extended research in this area. One aim of the researchers is to explore the effects of internal reinforcement in limit cases of adequate FRP strengthening of square columns for monotonic or cyclic loading. Another aim is to look into the influence of increases to the volumetric ratio of transverse reinforcement on the slenderness of bars, as well as the effect of monotonic and repeated loading – unloading (Rousakis & Karabinis 2012).

A Modified Confinement Ratio (MCR) as a measure of confinement effectiveness was proposed by Mirmiran et al. (1998).

$$MCR = \left(\frac{2r}{b} \right) \left(\frac{f_{le,FRP}}{f_{co}} \right) \quad (2.3)$$

Where,

b = the external dimension of the concrete section

r = the corner radius

$f_{le,FRP}$ = the maximum effective confining pressure provided by FRP for use on circular and rectangular rc confined with FRP, and

f_{co} = the compressive strength of unconfined specimen.

In accordance with the above study, Mirmiran et al. (1998) determined that specimens with $MCR < 0.15$ display inelastic softening stress-strain behaviour (with degrading branch).

Rousakis and Karabinis (2012) performed an experimental program using columns made of extremely low strength concrete with internal steel reinforcement and external FRP strengthening. The experiments concerned a series of tests of 42 prismatic columns of square cross-section, with 200 mm sides, 30 mm corner radius and 320 mm height. The height to side ratio was only 1.6 owing to restrictions of the available compression machine. The

specimens were reinforced with four longitudinal steel bars (volumetric ratio of 1.57%). Transverse steel stirrups of 8 mm diameter with 200 mm spacing (symbolized as S1) or 95mm (symbolized as S2) supported the bars, and thirty-two specimens were tested with FRP confinements using two types of unidirectional FRP sheets which were carbon S&P C240 or glass S&P G90/10 (S&P – Sintecno 1999). Rousakis and Karabinis found that plain concrete columns strengthened by a jacket with a ratio $MRC = 0.184$, revealed a slightly mechanical behaviour with softening branch. In columns with slender bars, a softening branch results an inadequate load response for $MRC = 0.153$ or lower. In those cases, the jacket could not confine the unsteady expansion of concrete thus, not exhibit a hardening inelastic behaviour. Also, the loading history of gradually increasing load–unload cycles resulted in further degraded responses for the columns. FRP strengthened columns with low s/Φ_L of the longitudinal bars and heavy steel stirrup confinement (non-slender bars, S2) under cyclic loading displayed strong upgraded mechanical behaviour. Their response was greater compared to columns with slender bars (S1), or plain concrete columns subjected to cyclic loading. A lower bound ratio of $MCR = 0.153$ corresponded to an obviously adequate mechanical response. Even though there was no significant variation of the axial strain at failure between columns with slender and non-slender bars, higher strain was found in columns with non-slender bars. According to this study, a ratio $MRC = 0.185$ could serve as a lower bound value to identify adequately confined columns.

Liang, M. et al. (2012) conducted an experiment to identify the influence of specimen size on the axial behaviour of carbon fibre reinforced confined concrete cylinders. As shown in Table 5, 24 specimens were prepared with different diameters and CFRP thicknesses. Twelve of the specimens were confined with CFRP cylinders but the remaining 12 were not and the FRP sheets used in this test used a kind of unidirectional carbon fabric which had ultimate tensile strength of 3591 MPa, elastic modulus of 242 GPa, and thickness of 0.167mm. All these cylinders had a slenderness of 2. For the CFRP-confined cylinders, small and large sizes were wrapped with one and three CFRP sheets of 200mm, respectively, whereas medium-sized cylinders were wrapped with a CFRP sheet of 200mm width and two CFRP sheets of 100mm width. Small, medium-sized, and large cylinders were wrapped with one layer, two layers, and three layers of CFRP, respectively. This study concluded that for a given lateral confinement no size effect existed in the normalised compressive strength gain f'_{cc}/f'_{co} and normalised ultimate strain $\epsilon_{cc}/\epsilon_{co}$ for the cylinders examined.

Table 5: Properties of concrete specimens

Specimen	Dimensions (mm)	Number of CFRP plies	Number of specimens
PC-S	$\Phi 100 \times 200$	0	4
CC-S	$\Phi 100 \times 200$	1	4
PC-M	$\Phi 200 \times 400$	0	4
CC-M	$\Phi 200 \times 400$	2	4
PC-L	$\Phi 300 \times 600$	0	4
CC-L	$\Phi 300 \times 600$	3	4

Source: Liang et al. 2012

Mohamed and Masmoudi (2010) conducted an experiment with 23 specimens. They applied many parameters. Five types of FRP tubes were used with different diameters and thicknesses. In these specimens, the following parameters were considered: concrete strength; thickness of FRP; the use of longitudinal steel bars; and slenderness ratio. From this experiment, the following results were reported:

- Increasing the thickness of FRP tubes resulted in a significant improvement of the strength and the ductility.
- For the CFT (Concrete-Filled FRP Tube) columns with steel reinforcement, the yielding of the steel bars was delayed by the confinement of FRP.
- In response to increasing the FRP volumetric ratio, the confinement strength increased at yielding as compared to the unconfined concrete compressive strength.
- The ultimate failure modes were different according to the specimen types A, B, and C which had thicknesses of 2.65mm, 2.85mm, and 6.40mm, respectively. For types A and B, it was very explosive, while the ultimate failure for type C was ductile.
- The ultimate load of the CFFT column with internal reinforcement was higher than without it.

2.7 Review of Analytical Studies – FRP Confinement

Xiao and Wu (2000) carried out an experimental program with 27 concrete cylinders confined by CFRP and developed a simple bilinear stress-strain approximation for confined concrete. This model was based upon empirical equations describing the axial stress-axial

strain and axial-stress transverse strain responses of the concrete tested. The model adopted the popular classical approach proposed by Richart, Brandtzaek and Brown (1928). The initial and final performances of these specimens were then modelled with two sets of linear equations using the four mechanical variables of: confined concrete; axial stress and strain; transverse strain; and confinement stress. These models were tested against the results of experimentation conducted by Hosotani, Kawashima and Kawashima (1996) and it was found that they modelled the data well, as shown in Figure 4.

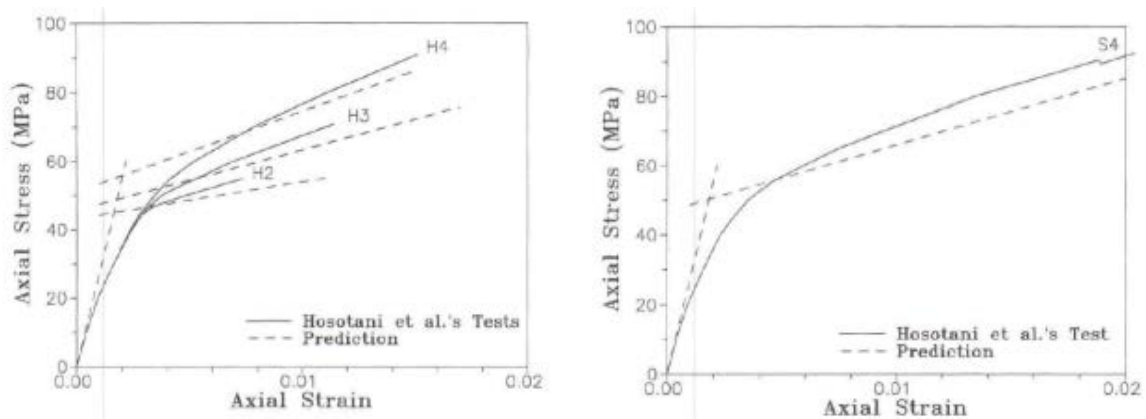


Figure 4: Bilinear simulation of Hosotani et al.'s test results

Source: Xiao & Wu 2000

Becque, Patnaik and Rizkalla (2003) performed numerical analysis using finite element models of the concrete confined with FRP composites to develop of stress-strain curves. A number of parametric comparisons were also conducted to see the effect of using various confinement materials, void sizes and numbers of fibre layers. Using the developed model, the normalised axial stress-strain curves for steel, CFRP and GFRP were found for a reinforcement ratio ρ of 1.6% with a concrete compressive strength of 35 MPa. The lower elastic modulus of GFRP allowed for greater strain to be developed, resulting in better ductility before column failure. The results indicated that an increase in the number of FRP layers increased confinement as well as ultimate strain. This led to an improvement in the ductility of the CFT columns tested.

Dandapat, Deb and Bhattacharyya (2011) pointed out that almost all numerical studies of FRP columns have not considered the failure of the bonding between the concrete column and the FRP tube. According to these researchers, after columns undergo degradation and damage during the loading process, de-bonding due to changes like relative tangential slip of normal gaps at the interfaces may be observed. Using an analytical expression following the

article shows the nature of the relationship between interfacial shear and fabric shear and strength:

$$\tau_i = \frac{K_{coh}\sigma_0}{E_c\sqrt{(a-b)}} \frac{\sinh(\sqrt{(a-b)}x)}{\sinh(\sqrt{(a-b)}L)} \quad (2.4)$$

According to these researchers, an interfacial shear stress depends on the wrap thickness, t , and Young's modulus of the wrap, E_f . Through Figure 5, it is shown that the interfacial shear stress increases from the fixed end to the axially loaded face of the column, and also increases with thickness of wrap and with Young's modulus of the wrap. Finally, they show that the interfacial shear stress is affected by the fabric thickness and generates increased debonding.

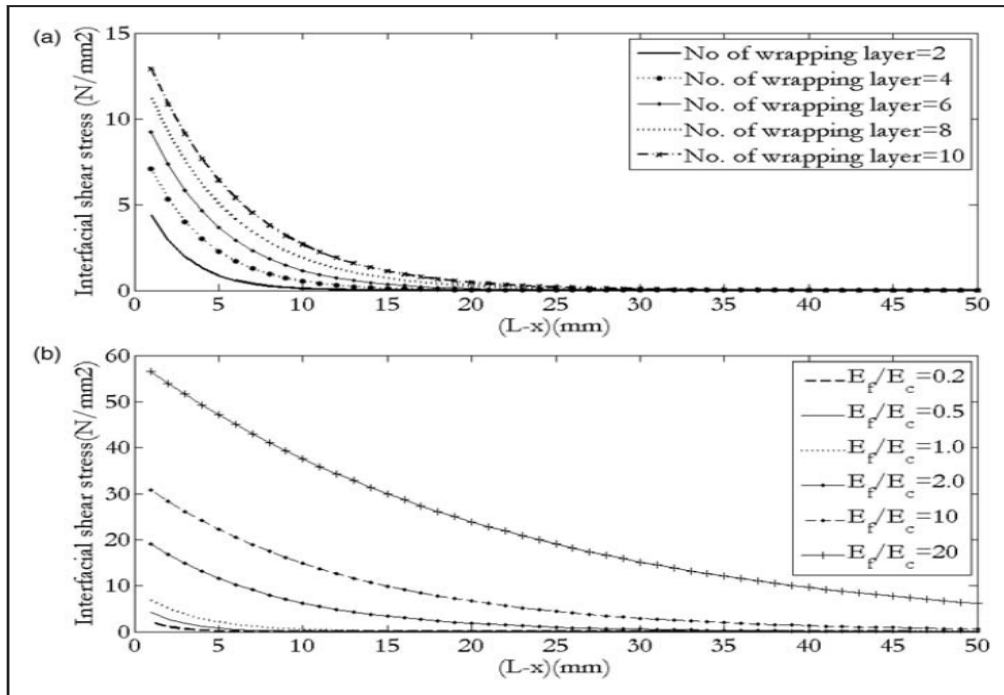


Figure 5: Variation of interfacial shear stress along the length of the column

(a) different wrap thickness values ($E_c=38$ GPa, $E_f=20$ GPa, $L=1.0$ m, and $K_{coh}=0.17E_f$; each layer of wrap is 0.5 mm); (b) different modular ratio ($E_c=38$ GPa, $L=1.0$ m, $t=1.0$ mm, and $K_{coh}=0.17E_f$).

Source: Dandapat et al. (2011)

The commercial finite element program ABAQUS was used for analysis of a more realistic numerical model of an FRP-confined concrete column. Two concrete cylinders were considered with different styles, one stocky and the other slender. Both were 150 mm in

diameter. Their heights were 350 mm and 1000 mm, respectively. Using the analytical model, it is known that there is a strong connection between failure in the bond and rupture in the fabric. That is, the damage to the bond between the fabric and the concrete results in significant effects on the failure load and ultimate strain.

2.8 Summary

The behaviour of CFT columns has been extensively studied for both steel and FRP confinement under various parameters and control measures to see what benefits FRP can introduce to current tube designs.

Results from these studies have confirmed the following characteristics of these columns that are applicable for both steel and FRP confined columns:

- Cross-sectional shape and column geometry have been shown to have a large impact upon the performance of CFT columns.
 - Square and rectangular columns have exhibited poor confinement with non-uniform confining pressure resulting in local buckling of the tube.
 - Failure of these columns has also resulted in undesirable wall bulging as opposed to the radial expansion failure of circular specimens.
 - Square and rectangular columns have also been shown to exhibit degrading stiffness and strain softening post-yield, whereas circular specimens exhibit strain hardening and are more ductile.
 - Generally circular columns have been shown to possess superior characteristics in virtually all areas as opposed to any other cross-sectional shape.
- It has been found that
 - CFT specimens with smaller D/t ratios (one study stated $D/t < 40$) experience significant lateral confinement pressure, higher ductility, higher flexural stiffness, higher buckling strength, higher axial strength, and better section interaction performance.
 - CFT specimens with larger D/t ratios have also been shown to fail by buckling before the concrete reaches a state of beneficial confinement pressure which increases compressive strength.
- This beneficial confinement characteristic was only seen in short columns, which generally possessed greater capacities than predicted.

- The compressive strength of the concrete core has also been observed to have large effects upon the behaviour of CFTs.
 - This has been shown through the interaction with varying aspect ratios as the benefits of confinement are reduced with an increase in concrete compressive strength.
 - One study showed that confinement of a medium strength (50 MPa) concrete mix occurred in tubes with D/t ratios ranging from 59 to 221 while a high strength (80 MPa) concrete mix resulted in confinement only at D/t ratios lower than 125.
 - Post-yield behaviour of higher strength concrete, especially with higher D/t ratios has been shown to result in strain softening.
 - Increased compressive strength results in higher stiffness and higher axial and moment capacities at the cost of a higher ratio of yield to ultimate stress and a reduction in mechanical efficiency, ductility, flexural stiffness, curvature ductility and section interaction performance.
- Several conclusions can also be drawn regarding the effect of confinement material properties:
 - It has been established that while steel confinement buckles and plastically deforms, the stress-strain curve of FRP composites and an experimental study indicates that these composite materials fail suddenly and in a brittle manner.
 - Stress-strain comparisons between steel and FRP also show that the confinement pressure of FRP increases until the first ply reaches failure, although for steel this pressure remains constant even after yielding under hoop tension.
 - It has been shown that for FRP confinement, an increase in the number of layers or ply of the confining tube results in greater confinement pressure, strength and ductility.
 - GFRP and CFRP composites have been tested almost exclusively and it has been found that GFRP is more ductile although not as strong in compression.

Chapter 3

METHODOLOGY

In order to achieve an understanding of the behaviour of concrete-filled FRP tubes, an experimental program was performed under uniaxial compressive load using 18 specimens with a variety of diameters and thicknesses to examine the behaviour of columns with different slenderness ratios. All testing was carried out at the civil engineering laboratory of the Central Queensland University. The primary test variable of the experimental program is the slenderness ratio of the FRP tube. Both concrete and FRP tubes were obtained from external providers. In this chapter, the objective of the experimental program is described as well as details of concrete-filled FRP tube specimens and material properties. For a better understanding of this experimental program, further information is added such as details of the instrumentation and test procedures that were used during the tests.

3.1 Objective of Experimental Program

The experimental program was designed to achieve the following objectives:

- Investigate the behaviour of FRP-confined tubes under uniaxial compressive load with varying slenderness ratios (Diameter (D)/Wall thickness (t) & Length (L)/ Wall thickness (t)),
- Investigate the failure mode of concrete-filled FRP tubes under uniaxial compressive load.

3.2 Design of Test Specimen

To achieve the abovementioned objectives, columns with varying diameters and wall thicknesses were selected. All specimens were circular columns, as circular tubes have

superior capacities compared to both rectangular and square ones due to their axis symmetric properties.

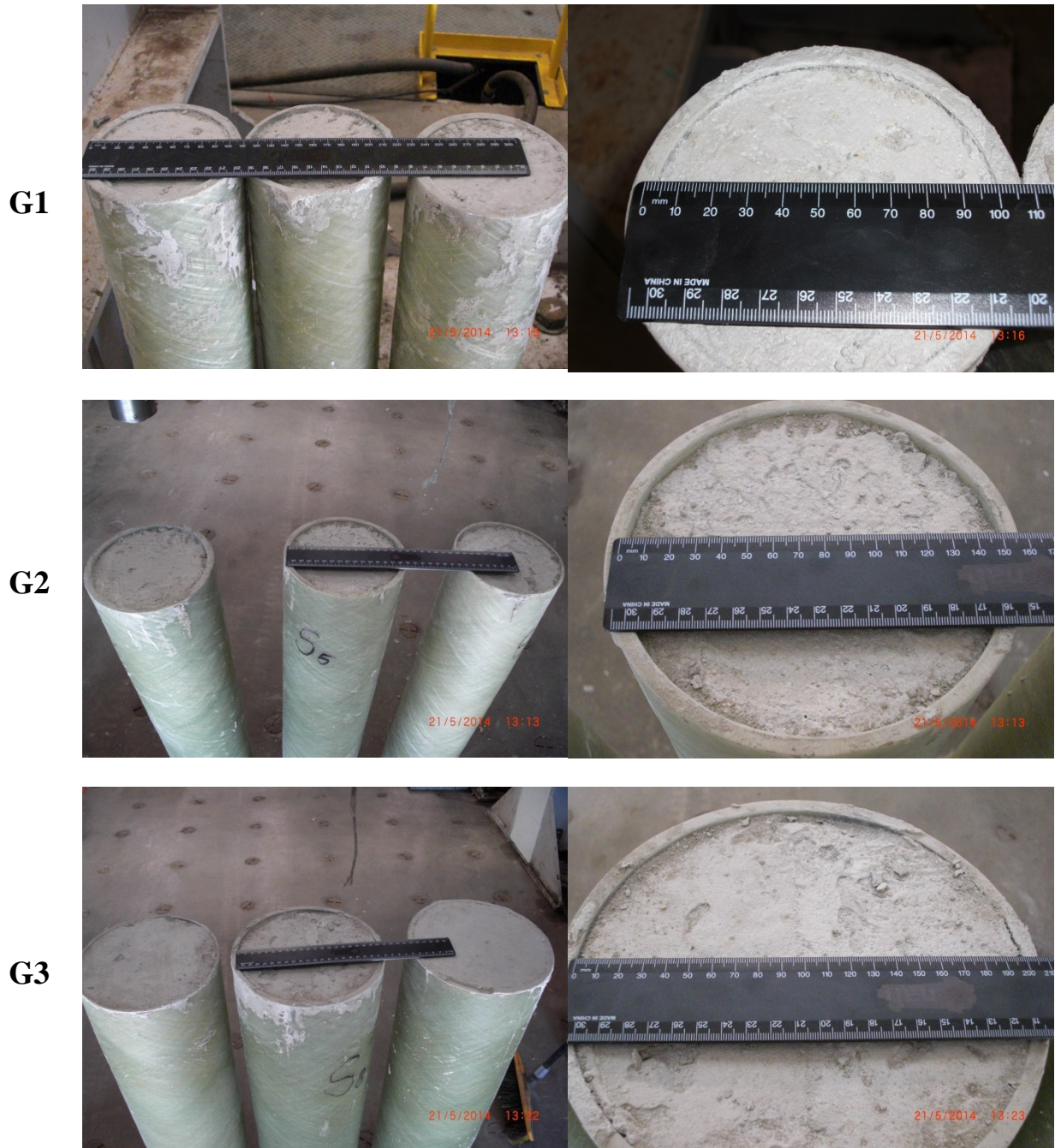


Figure 6: Groups of specimens according to the diameter of FRP tube

The length of specimens was kept constant at 1200 mm to save time with the practical set-up. The specimens were divided into three groups based on the outer diameter of the FRP tube.

Group 1(G1) – External diameter of the FRP is 100 mm

Group 2(G2) – External diameter of the FRP is 150 mm

Group 3 (G3) – External diameter of the FRP is 200 mm

In each group, three different wall thicknesses were selected: 3.5 mm, 8 mm and 9 mm. (Figure 6 shows these FRP tubes filled with concrete.)



Figure 7: FRP tubes with a variety of diameters and wall thicknesses

The wall thicknesses were selected in consultation with the manufacturer and there were not many options. As shown in Figure 7, in each group three different thicknesses were used. Two specimens were made with each group. That means total of 18 specimens were cast by pouring concrete into the FRP tubes. During the casting, concrete was poured into 3 layers and each layer was compacted as required. Prior to pouring concrete into the FRP tubes, the bottoms of the tubes were wrapped as shown in Figure 8 to prevent any leakage during the concreting because of the viscosity of the concrete. **Error! Reference source not found.**



Figure 8: Wrapped FRP tubes

In Table 6, the details of the specimens are listed. Specimens were divided into three groups according to their diameter and each group had six specimens with three different wall thicknesses as shown. In this table, it is shown that the specimens had a variety of D/T and L/T ratios. These ratios are primary factors in investigating the behaviour of concrete-filled FRP tubes. In the results chapter, the outcomes of this experiment are analysed mainly in terms of changes to the two types of ratio.

Table 6: Details of specimen (as per initial plan)

Group	Specimen	Inner Diameter (mm)	Wall thickness (mm)	Length (mm)	<i>D/t</i> ratio	<i>L/D</i> ratio
G1	D100T3A	100	3.5	1200	28.57	12.00
	D100T3B	100	3.5	1200	28.57	12.00
	D100T8A	100	8.0	1200	12.50	12.00
	D100T8B	100	8.0	1200	12.50	12.00
	D100T9A	100	9.0	1200	11.11	12.00
	D100T9B	100	9.0	1200	11.11	12.00
G2	D150T3A	150	3.5	1200	42.86	8.00
	D150T3B	150	3.5	1200	42.86	8.00
	D150T8A	150	8.0	1200	18.75	8.00
	D150T8B	150	8.0	1200	18.75	8.00
	D150T9A	150	9.0	1200	16.67	8.00
	D150T9B	150	9.0	1200	16.67	8.00
G3	D200T3A	200	3.5	1200	57.14	6.00
	D200T3B	200	3.5	1200	57.14	6.00
	D200T8A	200	8.0	1200	25.00	6.00
	D200T8B	200	8.0	1200	25.00	6.00
	D200T9A	200	9.0	1200	22.22	6.00
	D200T9B	200	9.0	1200	22.22	6.00

Note: D/T = Diameter/Wall thickness L/D = Length/Diameter

3.3 Material Properties

3.3.1 Concrete

Concrete was prepared by ordering from a ready-mix concrete supplier and all 18 specimens were filled with identical concrete with the following properties:

- Slump = 80 mmcm
- 20 mm nominal size aggregate
- Compressive strength = 32 MPa.

While the specimens were cast, a slump test was performed and, the compressive and tensile strengths of the concrete were also measured at the time of the testing. Slump of the fresh concrete was tested to measure the workability of concrete (Figure 9). The compressive strength of the concrete is shown in Figure 10). All tests were conducted as indicated using the Australian Standard AS 1012-1981 (Standards Australia 1981). As some of the AS 1012 standards have been altered since the introduction of the standards, the tests were performed in accordance with the revised versions as follows:

- Sampling of fresh concrete: AS 1012.1 – 1993
- Indirect tensile strength of concrete: AS 1012.10 – 2000
- Compressive strength of concrete: AS 1012.14 – 1991.



Figure 9: Slump test of concrete



Figure 10: Compressive strength test

All cylinder tests were conducted on the same day as the respective column tests and the results are summarised in Table 7.

Table 7: Compressive strength of concrete

Number	Load of failure (kN)	Compressive Strength (MPa)
1	210.7	26.93
2	275.2	35.18
3	235.8	30.39
4	215.6	27.56
5	228.8	29.25
6	260.1	33.25

3.3.2 FRP Tubes

Each FRP tube was manufactured by an external supplier. The properties of these tubes are listed in Table 8.

Table 8: Properties of FRP tubes

	Inner Diameter (mm)	Thickness (mm)	Elastic Modulus (axial) (MPa)	Ultimate Tensile Capacity (kg)	Stiffness (N/m/m)
100NB	101.7	3.5	8,816	10,670	30,005
	101.7	8		27,810	413,468
	101.7	9.5		33,830	685,948
150NB	153	3.5		15,840	9,114
	153	8		40,740	130,793
	153	9.5		49,350	219,809
200NB	203	3.5		20,980	3,967
	203	8		53,600	58,105
	203	9.5		64,780	98,294

3.4 Instrumentation

During the test, several instruments were used to record the behaviour of the specimens. The tests measured the loads, displacements and strains in the outer surface of FRP tubes filled with concrete.

3.4.1 Load Measurement

Load cell was used to measure the applying load. In this research, the facilities at Central Queensland University shown in Figure 11 were used. The tests were conducted using a uniaxial load machine (model HCC200) and details are given in Table 9.



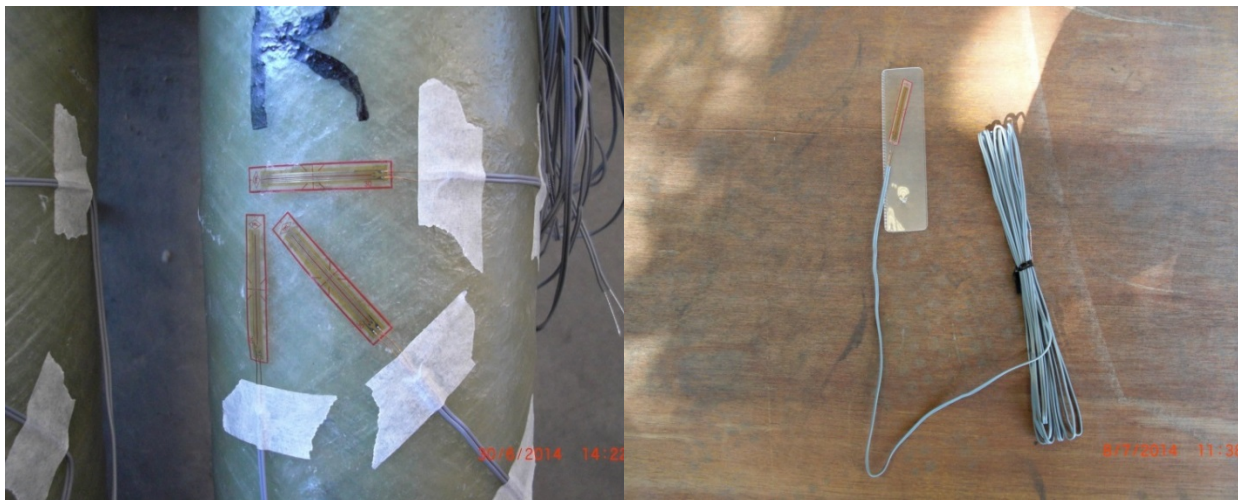
Figure 11: Uniaxial loading machine

Table 9: Specification of HCC200 load cell

Parameter	Value
Capacity	200 tonnes
Excitation	15 mv/V
Input resistance	700.0000 ohms \pm 10%
Output resistance	700.0000 ohms \pm 1%

3.4.2 Strain Measurement

Strain gauges 30 mm in length were used to measure the variation of strain. PEL-30-11 gauges were used and they had a gauge resistance of 119.6 (± 0.5) Ω and a gauge factor 2.11 (± 1) %. In total six strain gauges on two opposite surfaces in each specimen were attached in three directional positions (Figure 12).



(a) Strain gauge location on the FRP surface

(b) 30 mm Strain gauge

Figure 12: Strain gauges attached to the FRP tube

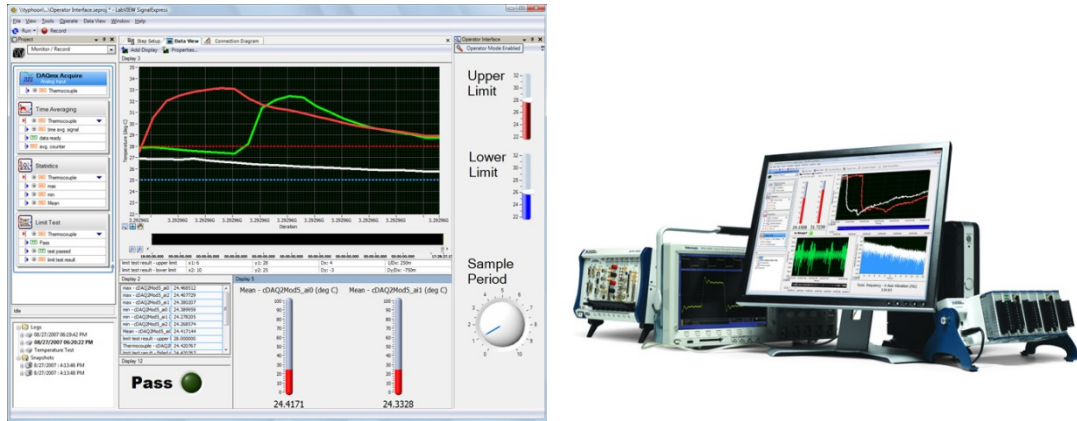


Figure 13: Measurement system instrument (Signal Express & NI 9219)
(Source - <http://www.ni.com/labview/signalexpress/whatis.htm>)

Signal Express is a data-logging software package for quickly acquiring, and presenting data with no programming required. After a series of steps involving the answering of questions the software writes the program in the background. A National Instruments compact DAQ chassis was used with four channel NI9219 Modules (Figure 13). With the NI 9219, several signals can be measured from sensors such as strain gauges, RTDs, thermocouples, load cells, and other powered sensors. The channels are individually selectable as well. In addition, the NI 9219 uses six-position spring terminal connectors in each channel for direct signal connectivity and contains built-in quarter-, half-, and full-bridge supports.

3.5 Testing Procedure

3.5.1 Test Set-up

During the test an identical load was applied to all specimens, which was a monotonically increasing load applied using a displacement control method. As the specimens were designed as pin ended columns, the test procedure was relatively simple. Apart from the longitudinal deformations, buckling was one major focus of this test. By considering the buckling effect on the columns, the strain gauges were attached at the same height on the opposite side of the column. It was also essential in the setting up of the experiment that certain safety procedures were established to protect the staff during the application of the load on the columns. Since neither the top nor bottom ends of specimens were fixed, this could lead fatal accidents. In particular, it was necessary to ensure that the columns were exactly vertical (Figure 14).



Figure 14: Set-up the FRP Column

3.5.2 Testing of specimens

Among the FRP columns from D100T3A~D150T9B, 12 specimens with different wall thicknesses (3.5mm, 8.5mm, 9.0mm) were first tested. Load increases of 1mm/min were applied monotonically to each column until it yielded. While 18 specimens were originally set up for this experiment, only 12 specimens with diameters of 100mm and 150mm were tested due to the limitations of load cell capacity. Even though the load cell was able to apply a load of 200,000 kg, it was necessary to reinstall the frames that supported the load cell for applying loads of this magnitude. This would have taken more time and the budget did not allow this.

After curing the columns, it was found that some of them had an empty space on the top of the tube which was formed due to the contraction of the concrete. To avoid different conditions on the top surface of each column, these gaps were filled with mortar (Figure 15) so that the load would be applied to both the concrete and the FRP tube simultaneously in spite of the lack of cohesion.



Figure 15: Filling the gaps with mortar

3.6 Risk Assessment and Health and Safety Procedures

Work place health and safety is emphasised heavily in engineering laboratories at the Central Queensland University. As this experimental program involved a heavy loading machine and FRP, there were a number of safety issues involved.

Simple safety measures were observed for the construction and loading of the specimens. All recommended personal protective equipment (PPE) such as hats and safety glasses were worn when the specimens were loaded. Other pieces of PPE were worn for specific activities during the construction.

In addition to general PPE, additional safety precautions were taken to avoid any possible hazardous incidents:

- A steel cage was used to protect the staff from flying particles from the specimens in the event of sudden failure (Figure 16)
- A steel plate was used to distribute the load on the top surface equally (Figure 17)
- Timber was used to ensure the columns were perpendicular (Figure 17)



Figure 16: Steel cage



Figure 17: Steel plate and timber

3.7 Summary

In this chapter, the all preparations for this experiment were described and information on the main materials such as FRP and equipment were provided, along with their specifications. Most of the time devoted to conducting this experiment was assigned to making the specimens. The selection of the FRP manufacturer was the hardest part and there were not many options, as they only supply the products manufactured on their production lines. This meant that the diameters and thicknesses of the tubes were decided by the manufacturer

rather than the researchers. Another factor that affected this research was the condition of the facilities at Central Queensland University, as we needed to consider the capacity of the load cell and lab-environmental supports. More information such as data sheets related to the experiment can be found in Appendix A.

Chapter 4

EXPERIMENTAL RESULTS

This chapter presents the experimental results obtained by the testing 12 specimens in the civil engineering laboratory at the Central Queensland University, along with an assessment of these results. This experiment was performed under the conditions described in the previous chapter. Preparations included configuring specimens, manufacturing the columns and installing the measuring instruments on the surfaces of the columns.

The information from the compression tests is presented in association with descriptions of the failure modes of the specimens. The main focus of discussion in these results is the behaviour of the composite columns under uniaxial compression with a variety of aspect ratios such as D/t and L/D . The observation of buckling is another issue in this experiment.

4.1 Overview of the Results

Table 10 summarises the results of the experiment. This table reveals the increase in the strength of columns due confinement by FRP tubes on the surface of the concrete columns. The specimens are according several different criteria such as diameter, thickness and strength of materials.

In general, the strength of composite columns increases as D/t ratio decreases. In this experiment, the strength of FRP columns decreased as the L/D ratio (slenderness ratio) decreased, which indicated that higher slenderness ratios cause columns to buckle more easily. However, it is not possible to reach this conclusion with certainty as the last three tests with the specimens D150T8B, D150T9A and D150T9B did not continue until they failed. In particular, there was unexpected buckling during the testing with specimen D150T8A and D150T8B, which may due to sliding at the loading point.

Table 10: Summary of experimental results

Specimen	Diameter (mm)	Thickness (mm)	Concrete Strength (MPa)	Tensile Strength of FRP (kN)	FRP Colum		Remarks
					Ultimate- load(kN)	Ultimate- strength (MPa)	
D100T3A	101.7	3.5	30.83	104.6	320	36.8	Buckling
D100T3B	101.7	3.5	30.02	104.6	281	32.3	Buckling
D100T8A	101.7	8	30.83	272.5	481	50.9	Buckling
D100T8B	101.7	8	30.83	272.5	505	53.5	Buckling
D100T9A	101.7	9.5	30.83	331.5	594	61.2	Buckling
D100T9B	101.7	9.5	30.02	331.5	498	51.3	Buckling
D150T3A	153.0	3.5	30.02	155.2	663	34.5	Buckling
D150T3B	153.0	3.5	30.02	155.2	601	31.3	Buckling
D150T8A	153.0	8	30.02	399.3	901	44.3	S-line buckling, failure at the top
D150T8B	153.0	8	30.02	399.3	931	45.8	Small buckling, Excess the load capacity
D150T9A	153.0	9.5	30.02	483.6	928	44.8	Excess the load capacity
D150T9B	153.0	9.5	30.02	483.6	932	45.0	Excess the load capacity

4.2 Ultimate Behaviour of FRP Columns

4.2.1 Behaviour of the Specimens with 100 mm Diameter and 3.5 mm Wall Thickness

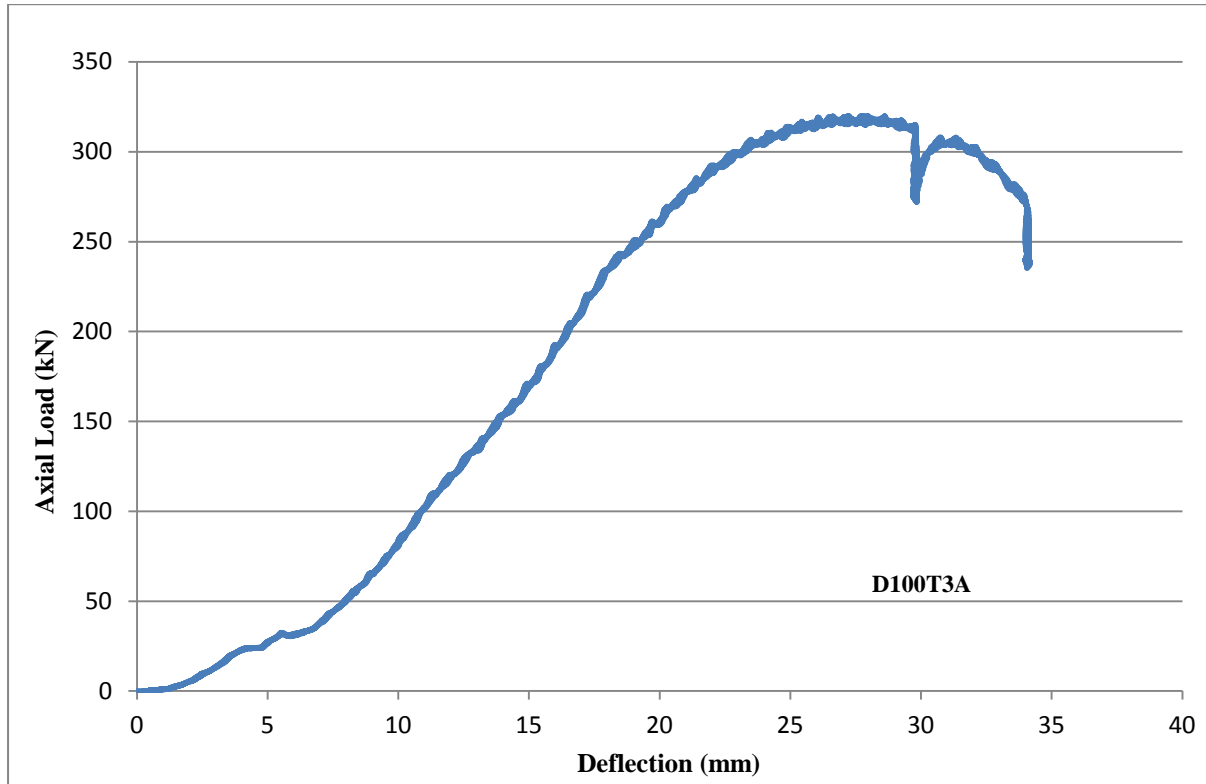


Figure 18: Load-deflection behaviour of specimens with 100 mm diameter and 3.5 mm wall thickness (D100T3A)

As explained in Chapter 3, the load on the columns was increased at a constant rate of 1 mm/min until their failure. During the loading, the load varied linearly with displacement until about 180 kN. At a load of about 180 kN, some changes were observed in the columns. The FRP tubes stretched and started to buckle. This was shown by texture changes in the middle part of the tube as shown in Figure 19.



Figure 19: Change of texture

After this point the column apparently started to bend in the vertical plane. However, no damage/fracture was observed in the outer surface. As loading continued, the column buckled and load started to decrease. After a drop of about 10% from the ultimate load, the load was removed. An ultimate load of 320 kN was recorded.

The behaviour of specimen D100T3A is revealed from analysing the strain variation on the external surface of the tube. As indicated in Chapter 3, a total of six strain gauges were attached to the column on two opposite sides, with three gauges on each side.

Initially, as shown in Figure 20, no significant strain variation was measured in any of the six strain gauges until the load reached about 180 kN, at which point the beginning of buckling was noticed. After this stage, highly increased strains are observed in the gauges attached in horizontal and longitudinal directions (X, Y), while the other gauges in the oblique direction (Z) show a steady increase in strain. The tensile stress can be calculated approximately from Equation 4.1, which is about 88.16 kg. Comparison with the ultimate tensile capacity of the FRP of 10,670 kg as mentioned in methodology shows that this is very far from the failure point.

$$\sigma_x = E\varepsilon_x \quad (4.1)$$

Where,

σ_x = Normal stress

E = Elastic Modulus

ε_x = Normal strain

Having similar variations in R1 and L1, and R2 and L2, it shows that the load applied on the top of the column distributed the hoop stress on the FRP tube equally.

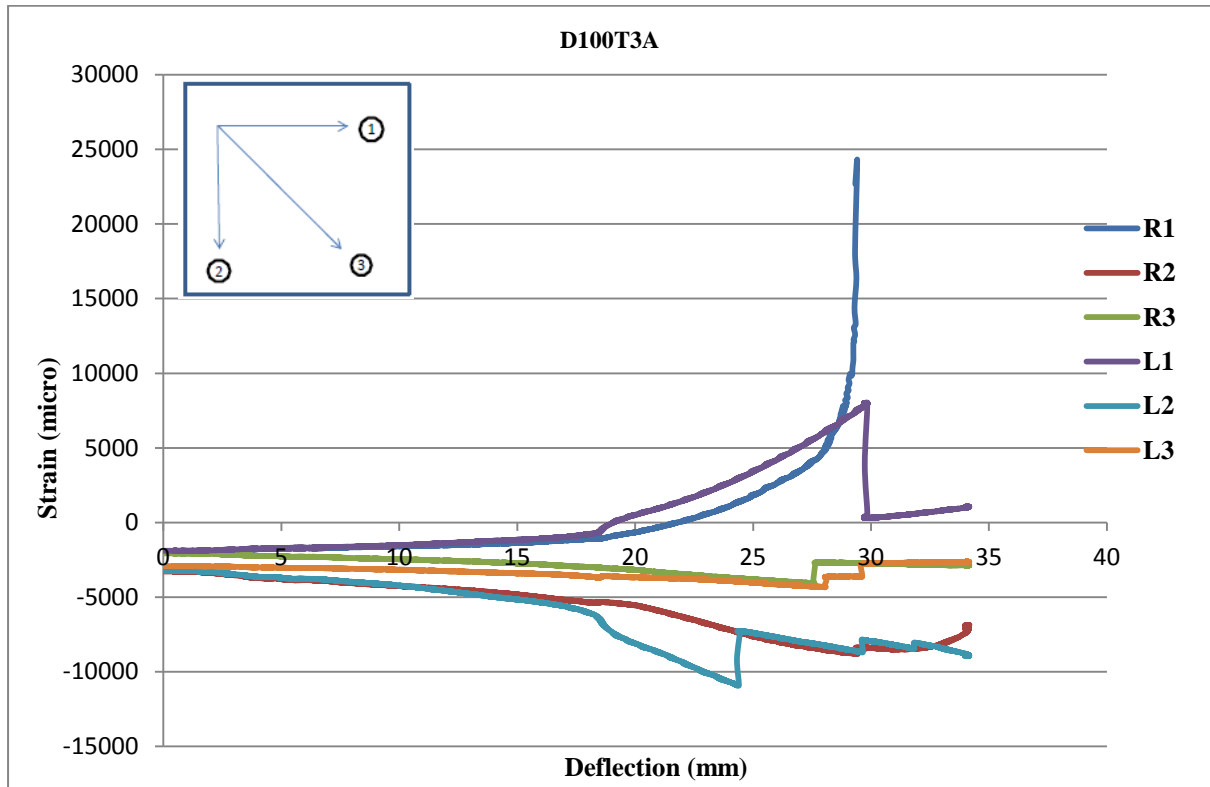


Figure 20: Strain-deflection behaviour of specimen D100T3A

Although the load-deflection behaviour of specimen D100T3B (Figure 21) showed a similar pattern to D100T3A, the ultimate stress was measured at the lower point, about 280 kN. At a load of nearly 250 kN, buckling was observed but no visible fracture was observed. This specimen exhibited slightly larger ductility than D100T3A.

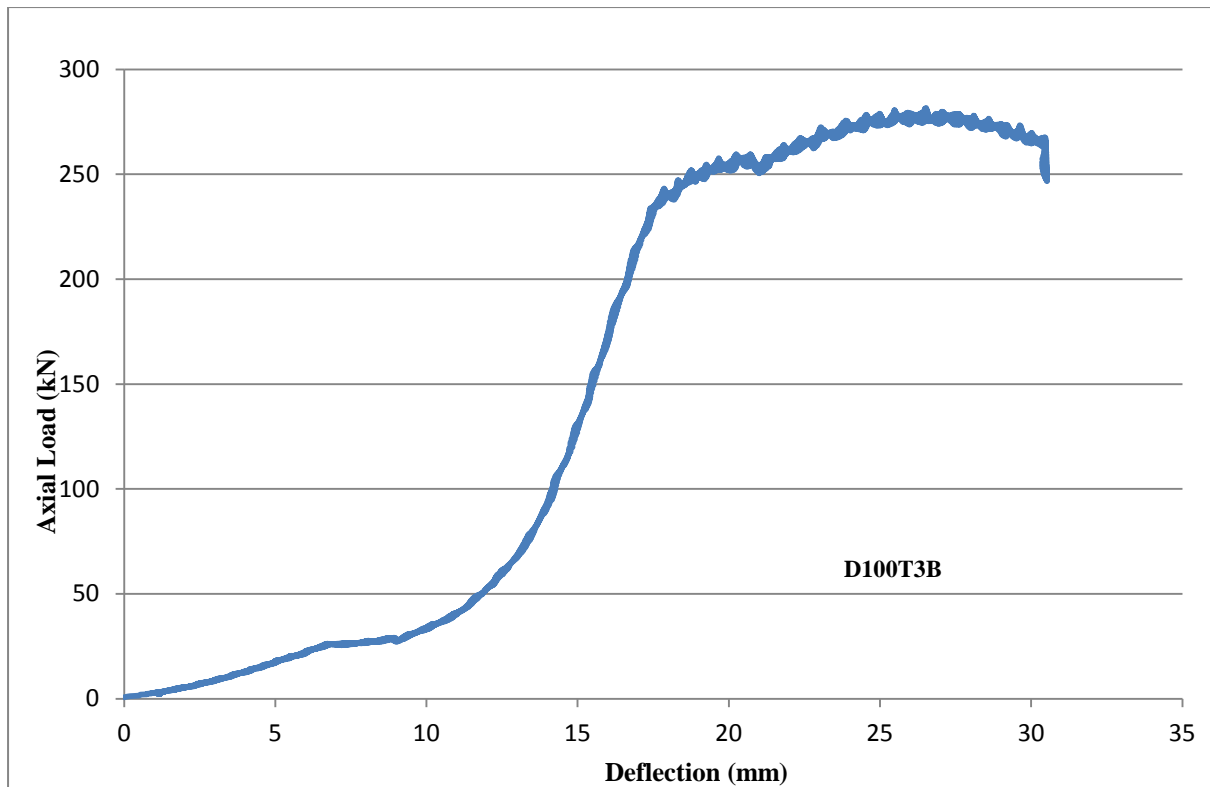


Figure 21: Load-deflection behaviour of specimen D100T3B

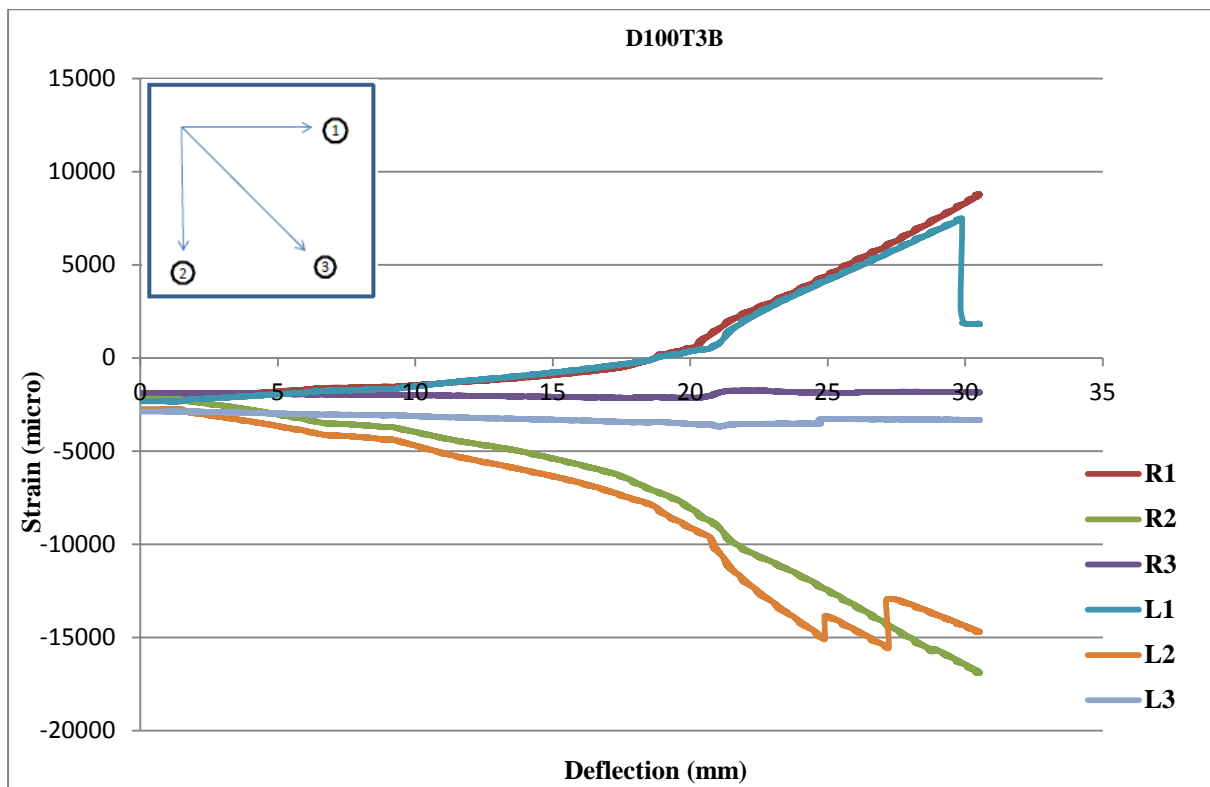


Figure 22: Strain-deflection behaviour of specimen D100T3B

Each pair of strain gauges for specimen D100T3B showed similar behaviour with strains in X and Y directions showing significant increases, from about 20 mm of deflection while the Z direction shows no changes as shown in Figure 22.

4.2.2 Behaviour of the Specimens with 100 mm Diameter and 8.0 mm Wall Thickness

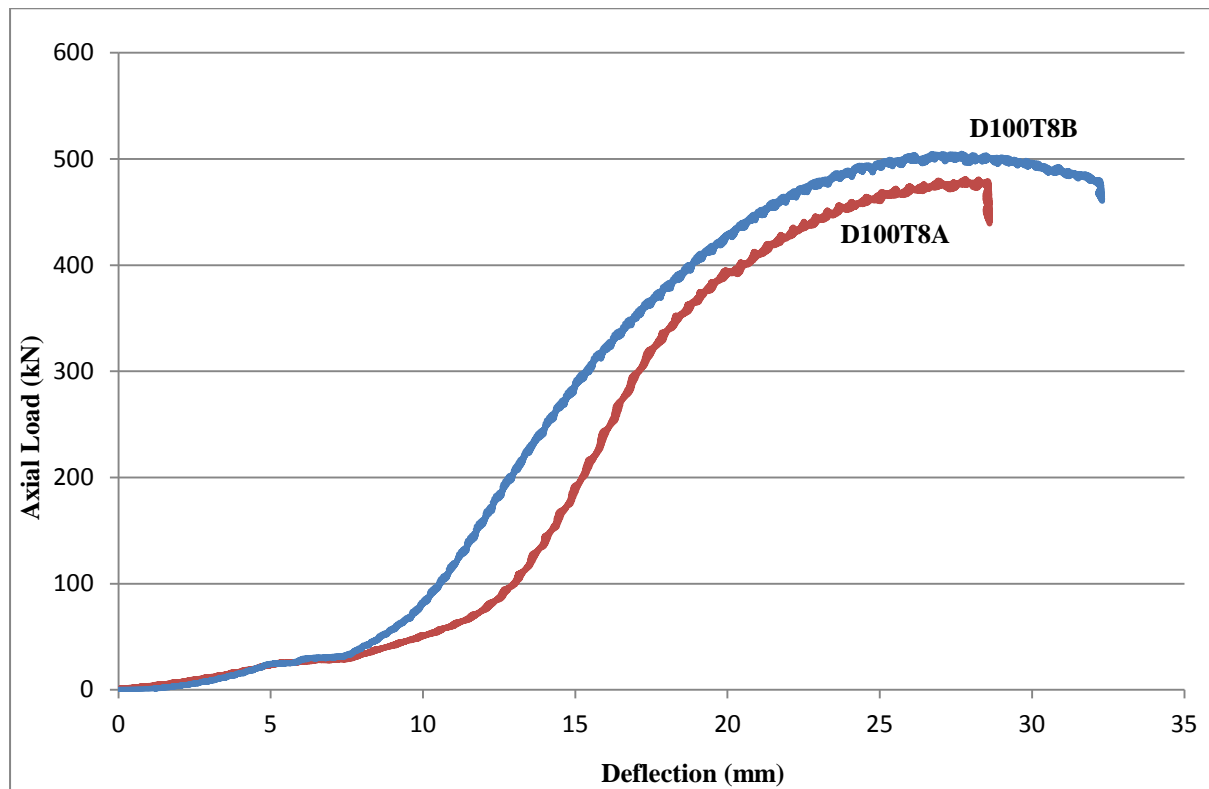


Figure 23: Load-deflection behaviour of specimens with 100 mm diameter and 8.0 mm wall thickness

As shown in Figure 23, D100T8A carried a higher ultimate load, about 480 kN and suddenly showed a drop in the load down without much ductility after the ultimate load. Until its ultimate load of 500 kN, similar load-deflection behaviour was observed in D100T8B as in D100T8A. However D100T8B exhibited slightly better ductility than D100T8A before failure. This variation may have been due to various factors such as loading pattern, and orientation of FRP in the tubes.

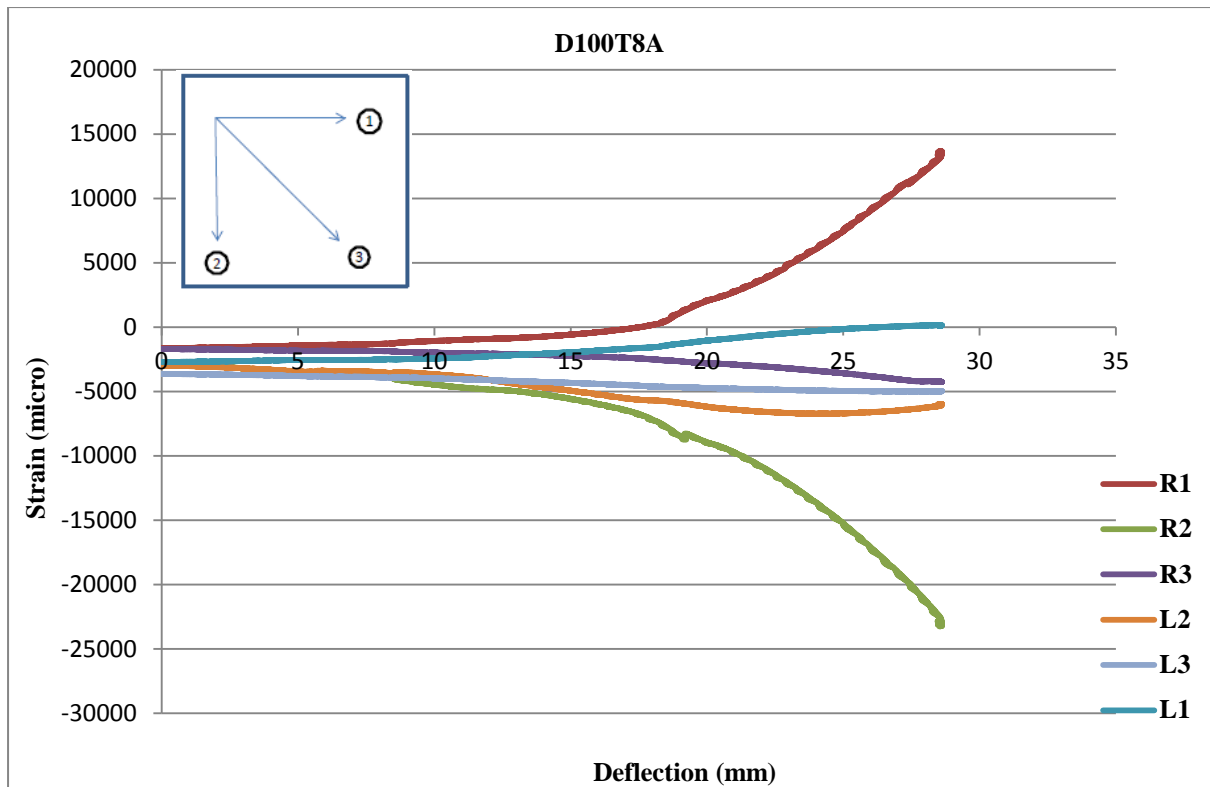


Figure 24: Strain-deflection behaviour of specimen D100T8A

The buckling of the specimens can be further confirmed by looking at the strain variation in the outer surfaces of the columns. Figure 24 shows the strain behaviour of specimen D100T8A, which reveals that R1, R2 increased considerably with 15 mm of deflection while the others showed only small changes. A similar pattern can be also seen in Figure 25, which shows the strain variation in the specimen D100T8B. When the strain increased rapidly, that means buckling occurred or started towards that side.

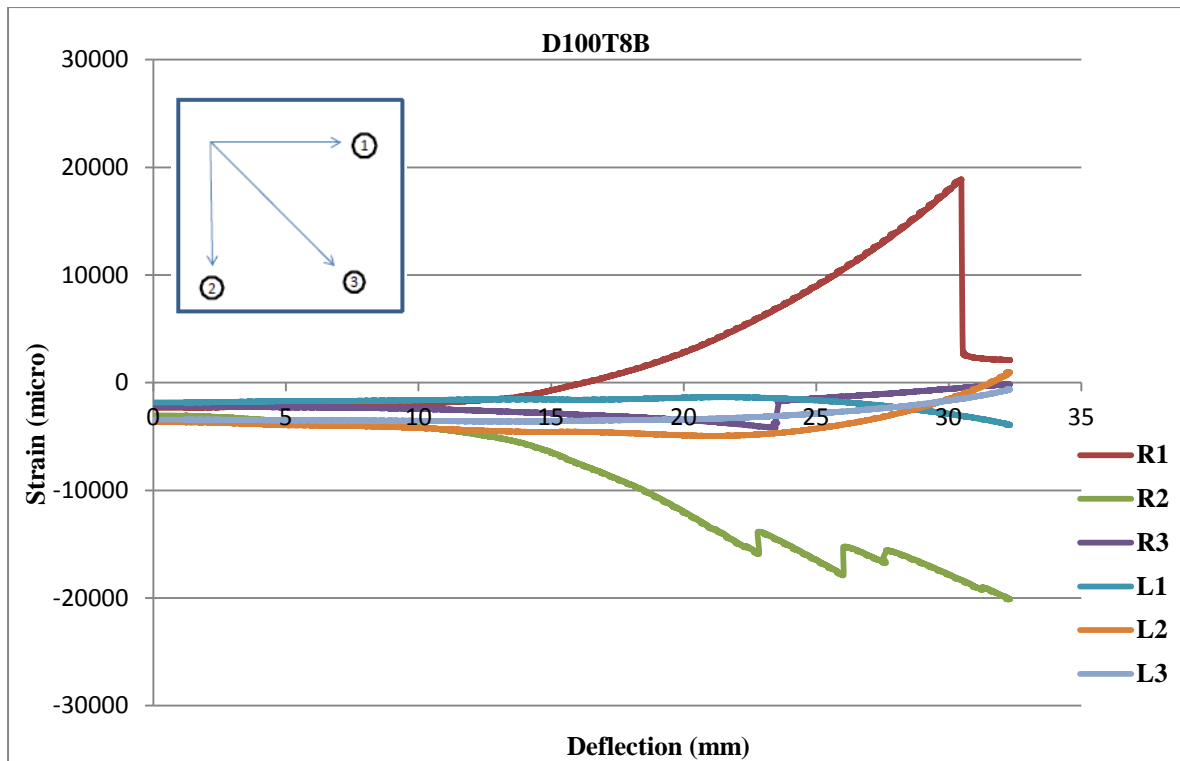


Figure 25: Strain-deflection behaviour of specimen D100T8B

4.2.3 Behaviour of the Specimens with 100 mm Diameter and 9.0 mm Wall Thickness

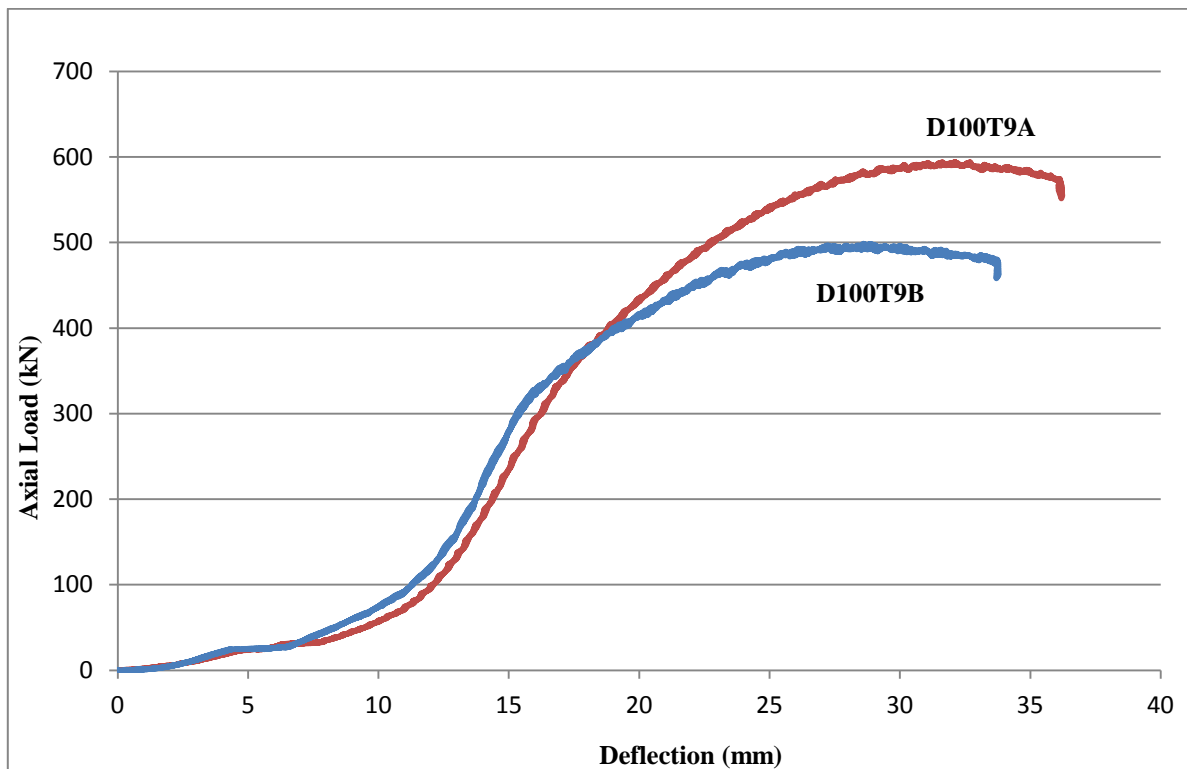


Figure 26: Load-deflection behaviour of specimens with 100 mm diameter and 9.0 mm wall thickness

Specimen D100T9A was the specimen with the thickest FRP tube and it recorded higher ultimate stress, almost 600 kN, than the other specimens. Load increased slowly until reaching 100 kN. This may be due mainly to seating errors in the specimen. After this point a steady nearly linear increase was observed until about 500 kN. Then the load increment dropped and it carried about 600 kN before the load dropped. Specimen D100T9B follows a similar path, as shown in Figure 26, but reached a slightly lower ultimate load of about 500 kN.

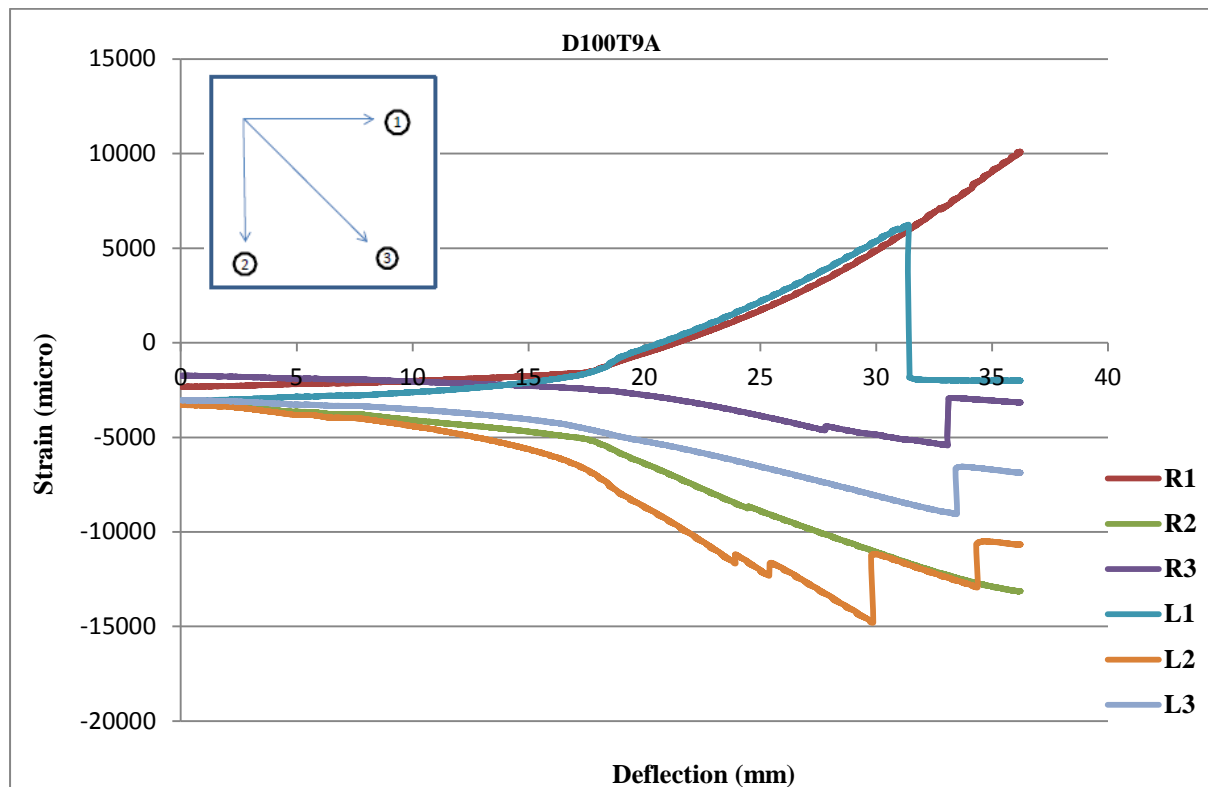


Figure 27: Strain-deflection behaviour of specimen D100T9A

Similar to former specimens, the variation in all strain gauges for D100T9A indicates that during the first 15 minutes of test time there was no significant change. However, after that, considerable movement was observed on every gauge. In the last part of test, all strain gauges were detached except R1 and R2 (Figure 27).

From about 7 mm of deflection in specimen D100T9B, strain-deflection behaviour increased variously as both X directional gauges show some increase and both Y directional gauges show significant contraction. With a change to a burred colour, D100T9B started buckling in the middle part of the column (Figure 28).

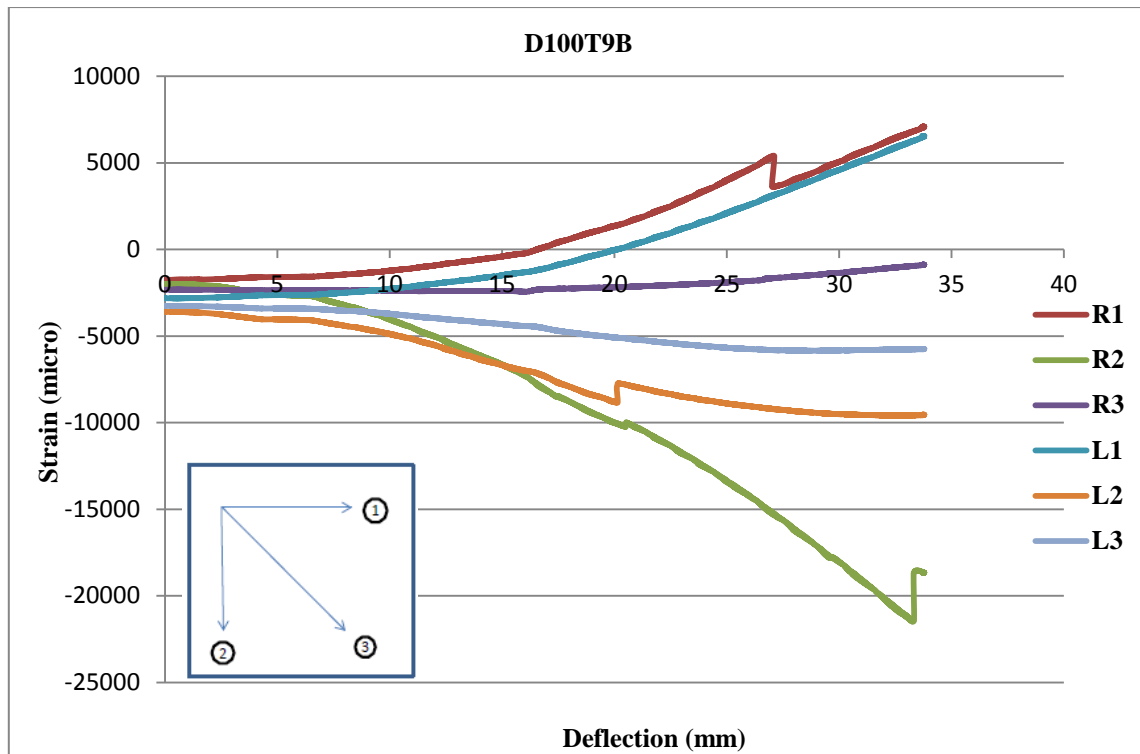


Figure 28: Strain-deflection behaviour of specimen D100T9B

4.2.4 Behaviour of the Specimens with 150 mm Diameter and 3.5 mm Wall Thickness

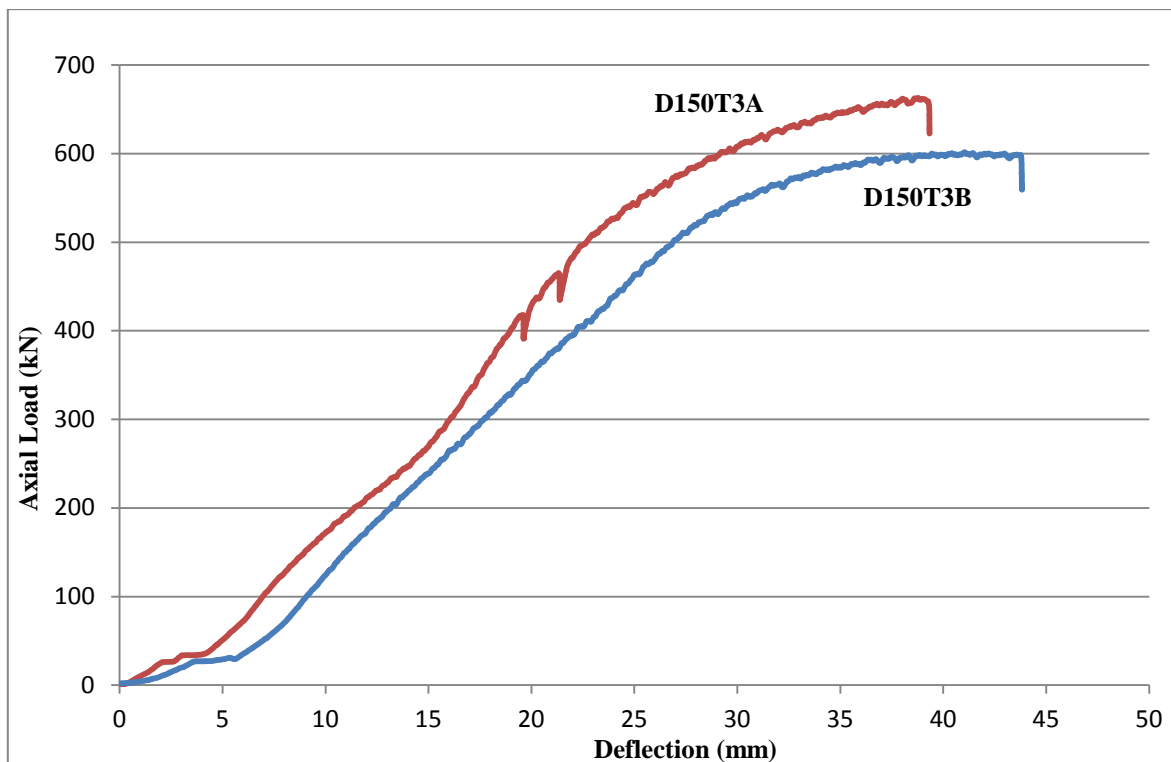


Figure 29: Load-deflection behaviour of specimens with 150 mm diameter and 3.5 mm wall thickness

Specimen D150T3A which was 150 mm in diameter, had a relatively high ultimate stress, and until its failure the axial load increased at a fairly constant rate (Figure 29). The load-deflection behaviour of specimen D150T3B showed a similar pattern to specimen D150T3A and the column failed when the load reached 600 kN.

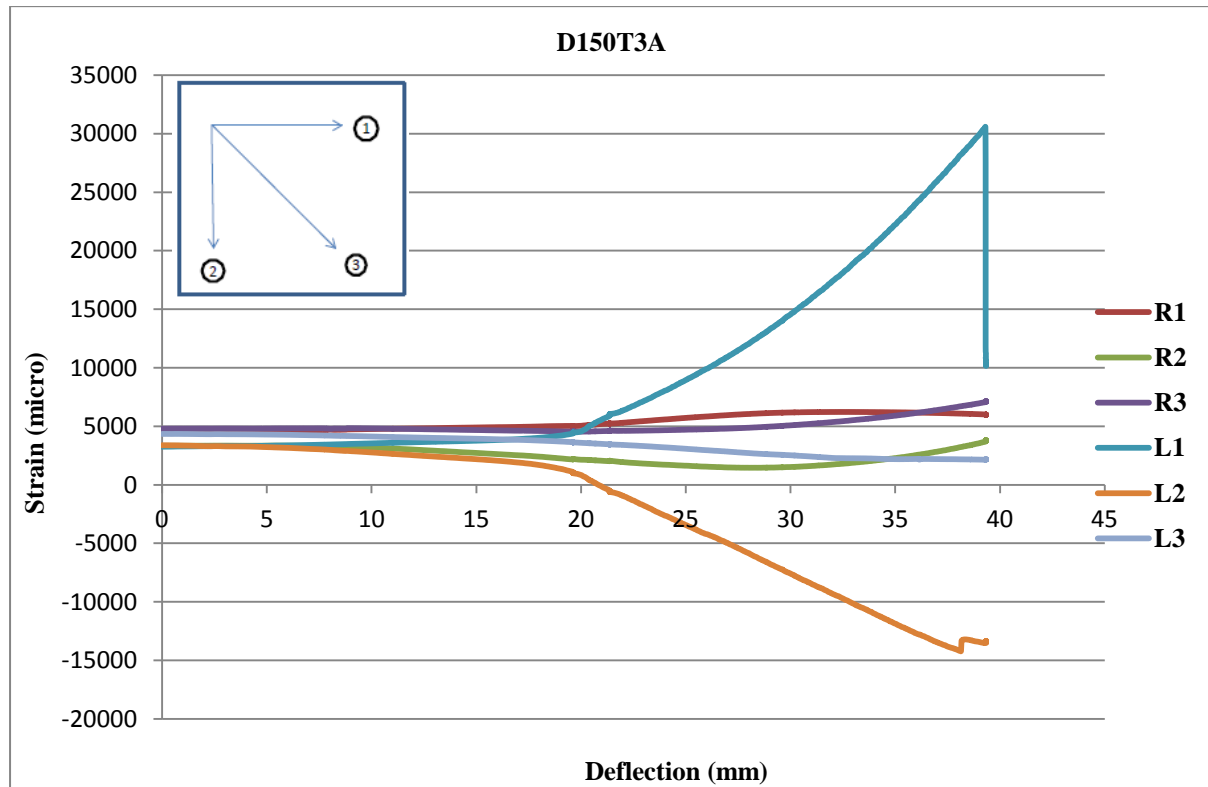


Figure 30: Strain-deflection behaviour of specimen D150T3A

The testing of specimen D150T3A showed some of the same strain-deflection behaviour as previous specimens as there is no significant variation until 20 mm of deflection appeared in all gauges. After that, however, the strain started stretching on gauge L1 along with contracting on L2 (Figure 30).

The strain-deflection behaviour of specimen D150T3B also showed a similar pattern to specimen D150T3A. There was no significant strain behaviour until it reached to 20 mm of deflection, then, both horizontal strain gauges recorded remarkable changes and one side of longitudinal appeared strain change (Figure 31).

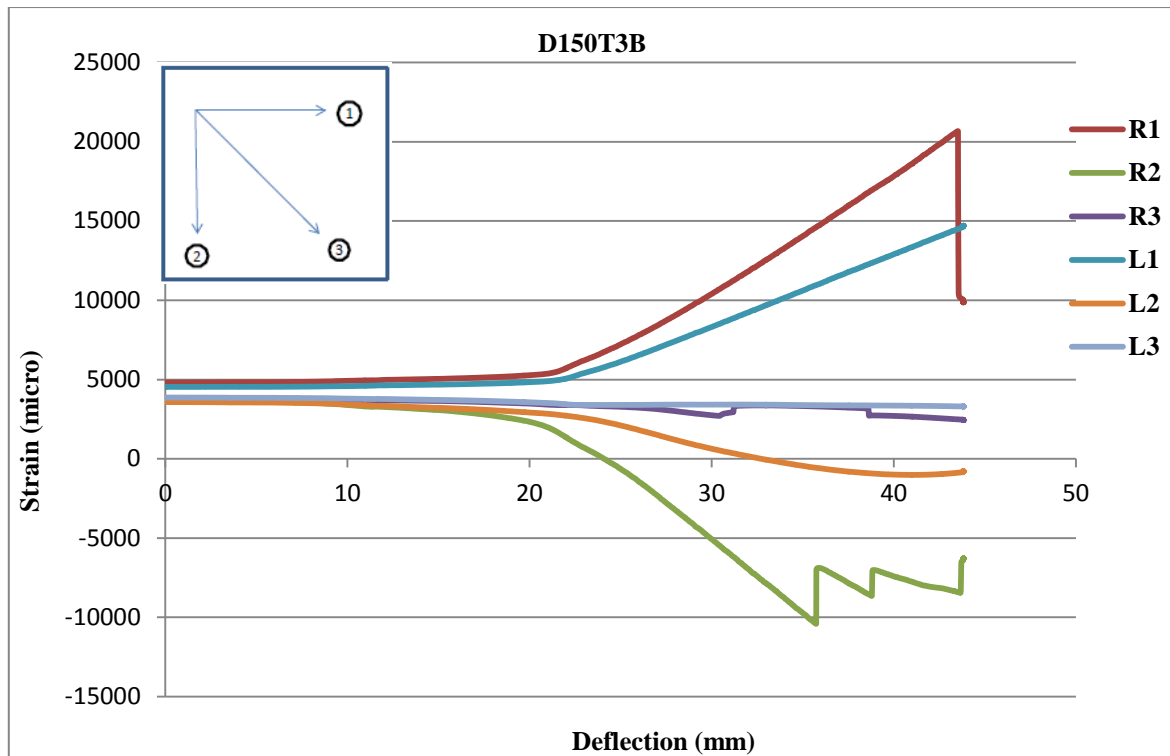


Figure 31: Strain-deflection behaviour of specimen D150T3B

4.2.5 Behaviour of the Specimens with 150 mm Diameter and 8.0 mm Wall Thickness

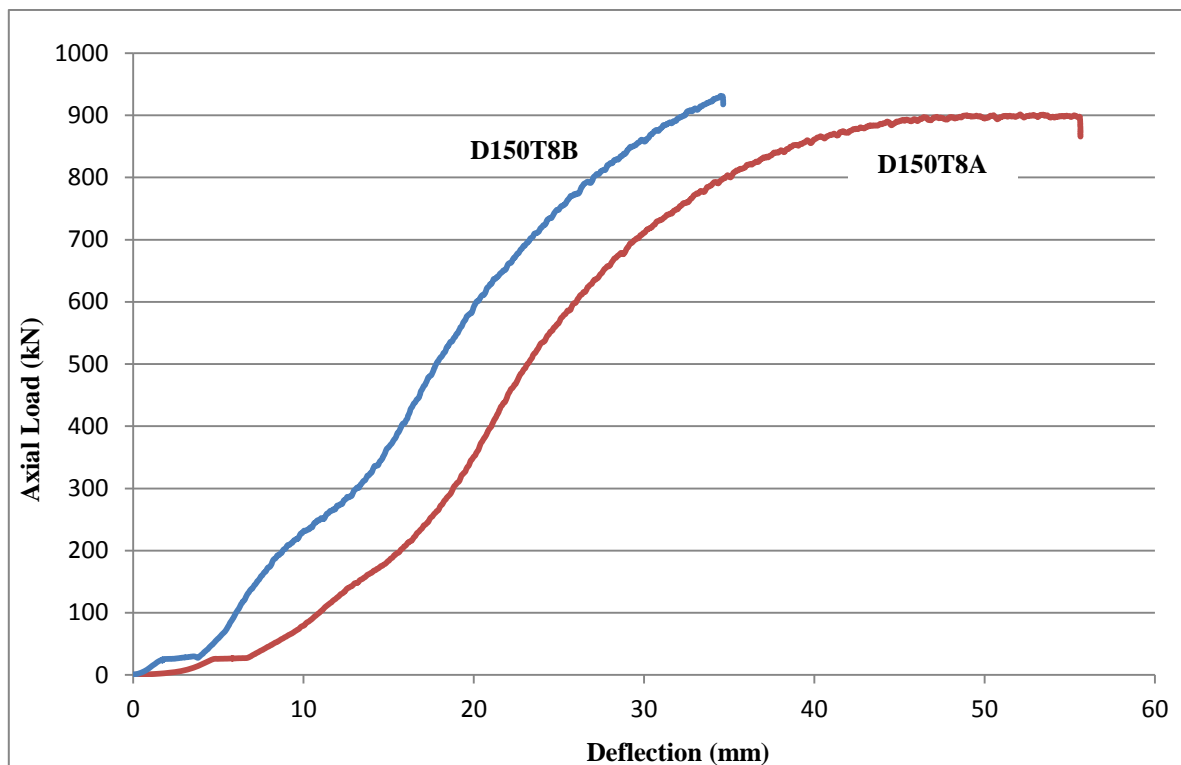


Figure 32: Load-Deflection behaviour of specimens with 150 mm diameter and 8.0 mm wall thickness

The ultimate stress of specimen D150T8A was recorded at over 900 kN during the test, which increased gradually from the initial time of test (Figure 32). S-line buckling was detected on this column, which occurred towards the top and bottom of the column whereas for most specimens buckling appeared at the middle of the column (Figure 33). Although axial load increased to over 900 kN in specimen D150T8B, it was necessary stop loading due to the limitations of the loading frame.

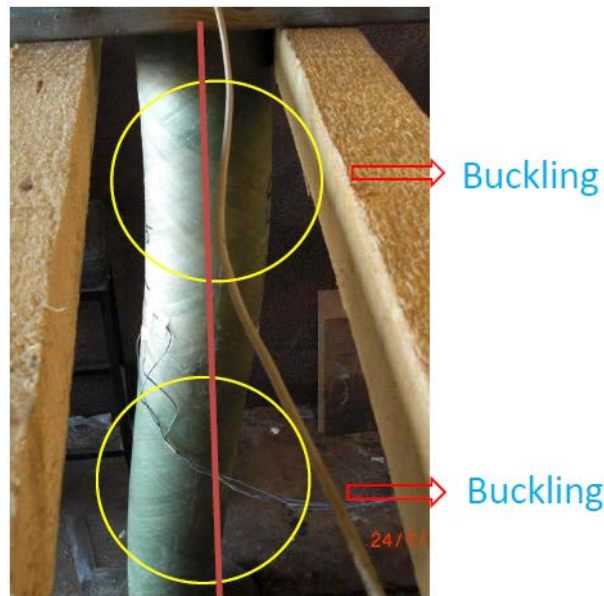


Figure 33: Buckling in specimen D150T8A

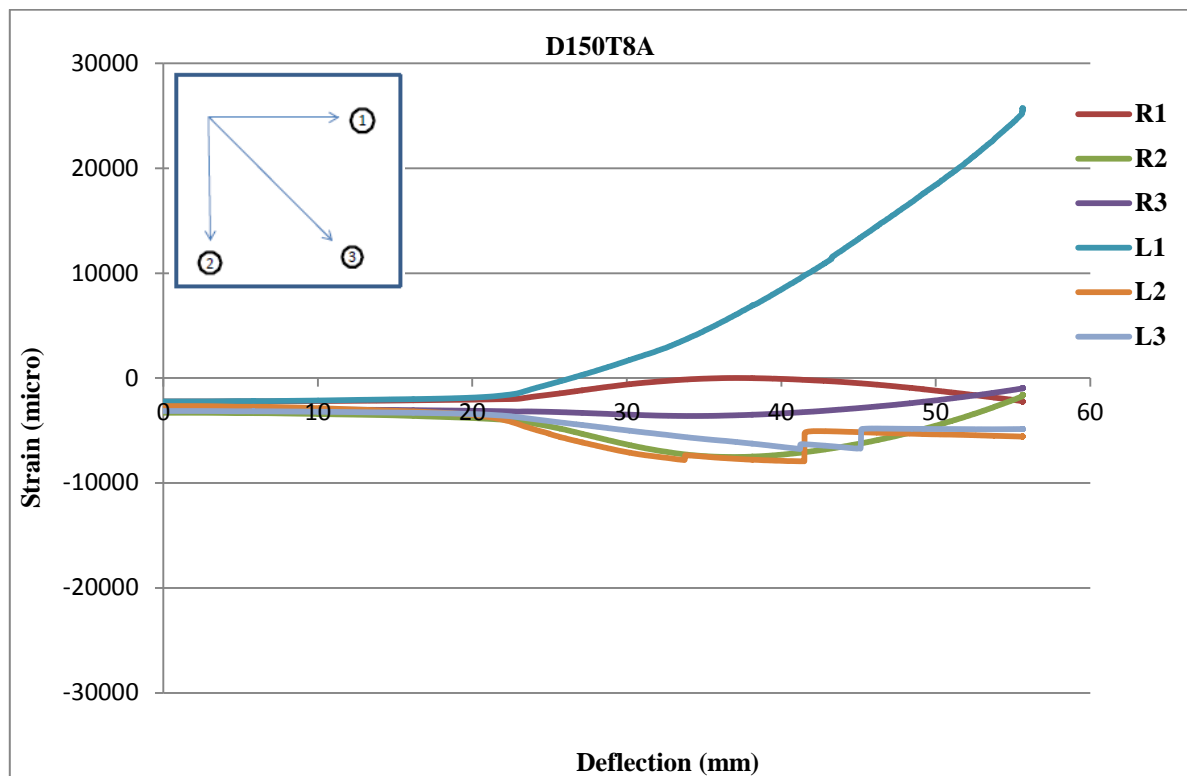


Figure 34: Strain-deflection behaviour of specimen D150T8A

In a similar way, all strain gauges showed no significant variation until the deflection reached 20 mm, and after that, L1 showed highly increased strain up to the failure (Figure 34 & Figure 35).

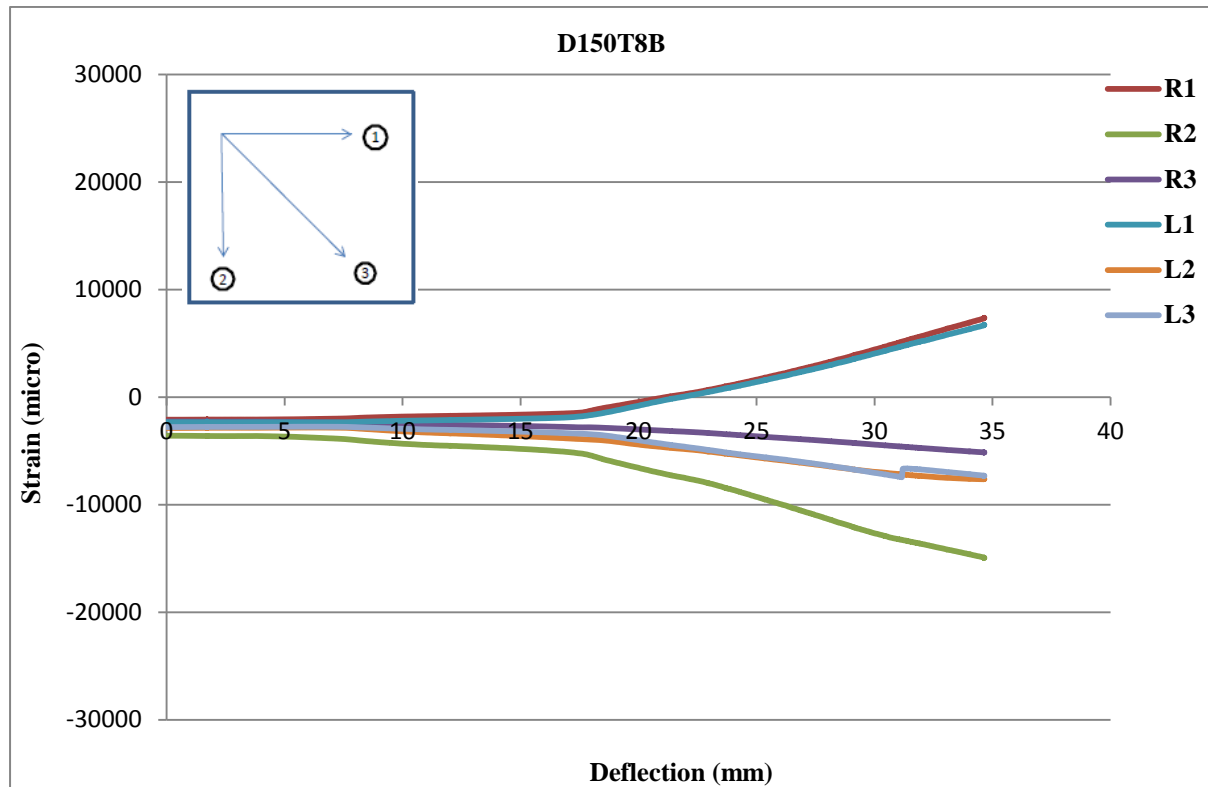


Figure 35: Strain-deflection behaviour of specimen D150T8B

4.2.6 Behaviour of the Specimens with 150 mm Diameter and 9.0 mm Wall Thickness

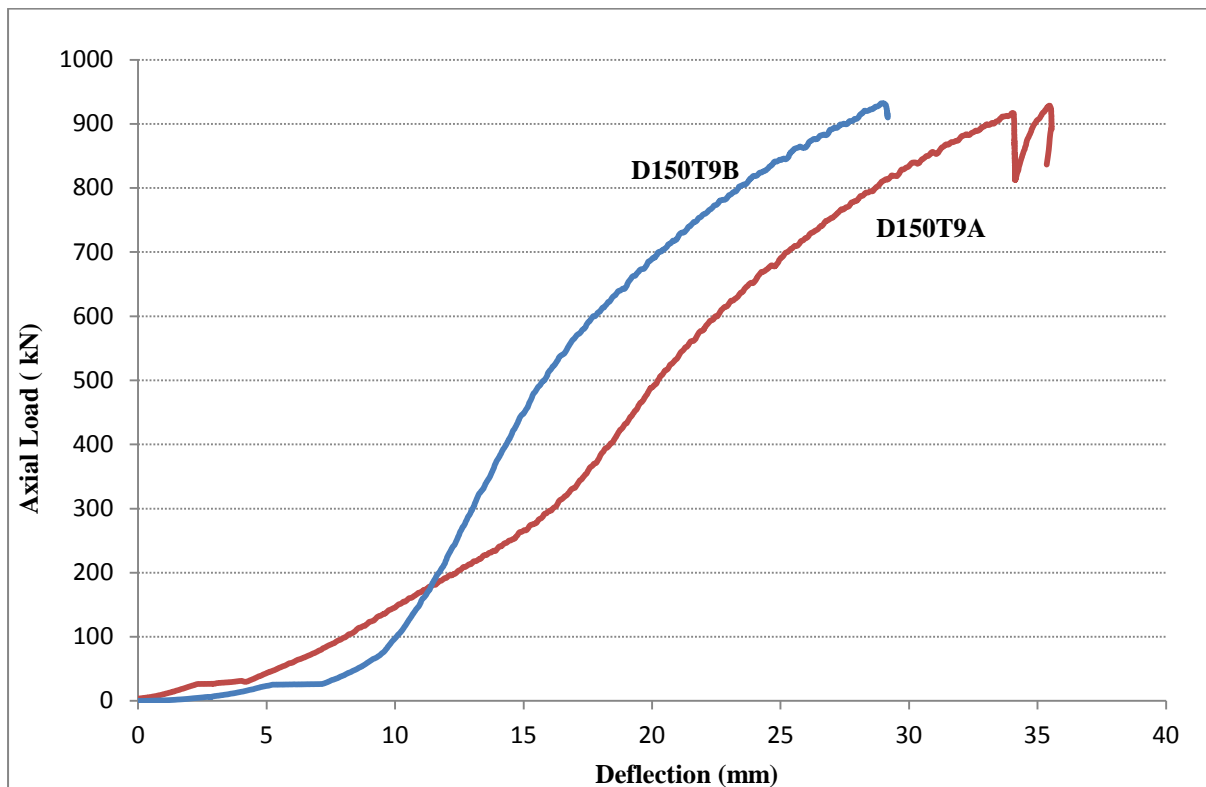


Figure 36: Load-deflection behaviour of specimens with 150 mm diameter and 9.0 mm wall thickness

As shown in Figure 36, during the initial stage of both tests, these two specimens displayed different behaviours under load. However, average features of loading behaviour mostly followed the same pattern. Due to the load cell limitations, further loading was not allowed in these specimens.

The pattern of strain in D150T9A resulted in active movements in all six gauges after approximately 20mm of deflection as shown in Figure 37. From this behaviour, it can be assumed that expansion occurred from inside of columns owing to the compression force which was applied without any buckling.

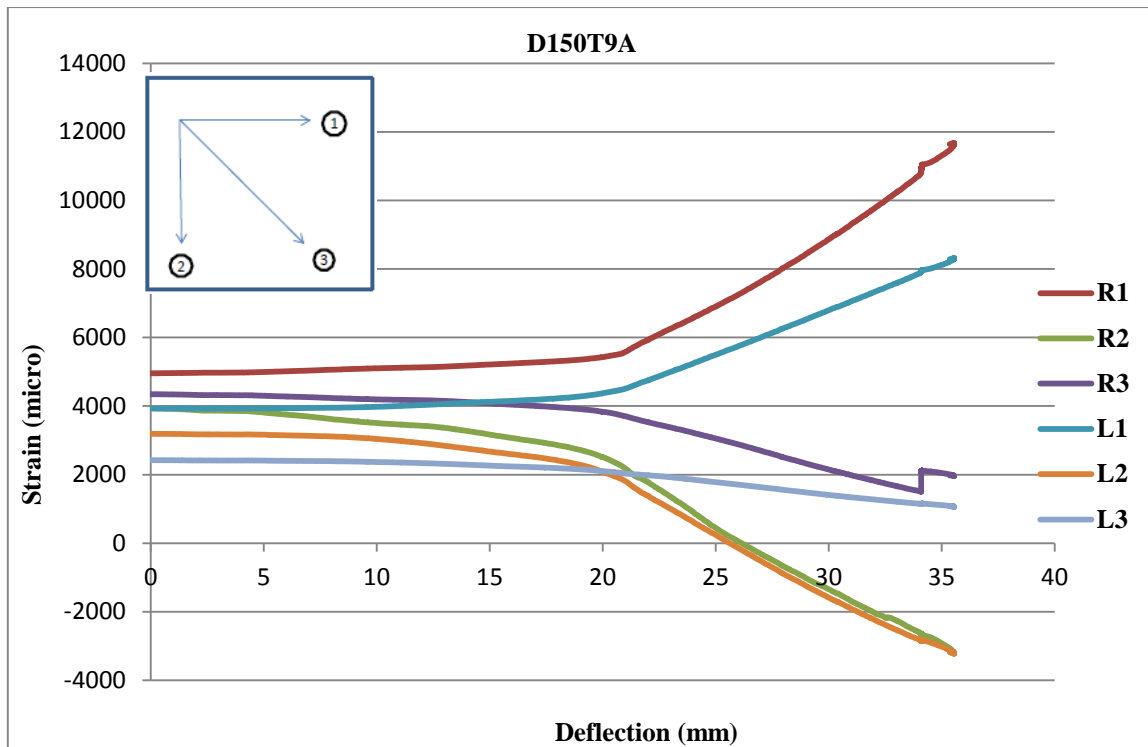


Figure 37: Strain-deflection behaviour of specimen D150T9A

The strain gauges in Specimen D150T9B showed similar behaviour to D150T9A, and movements developed at the point of approximately 15mm of deflection.

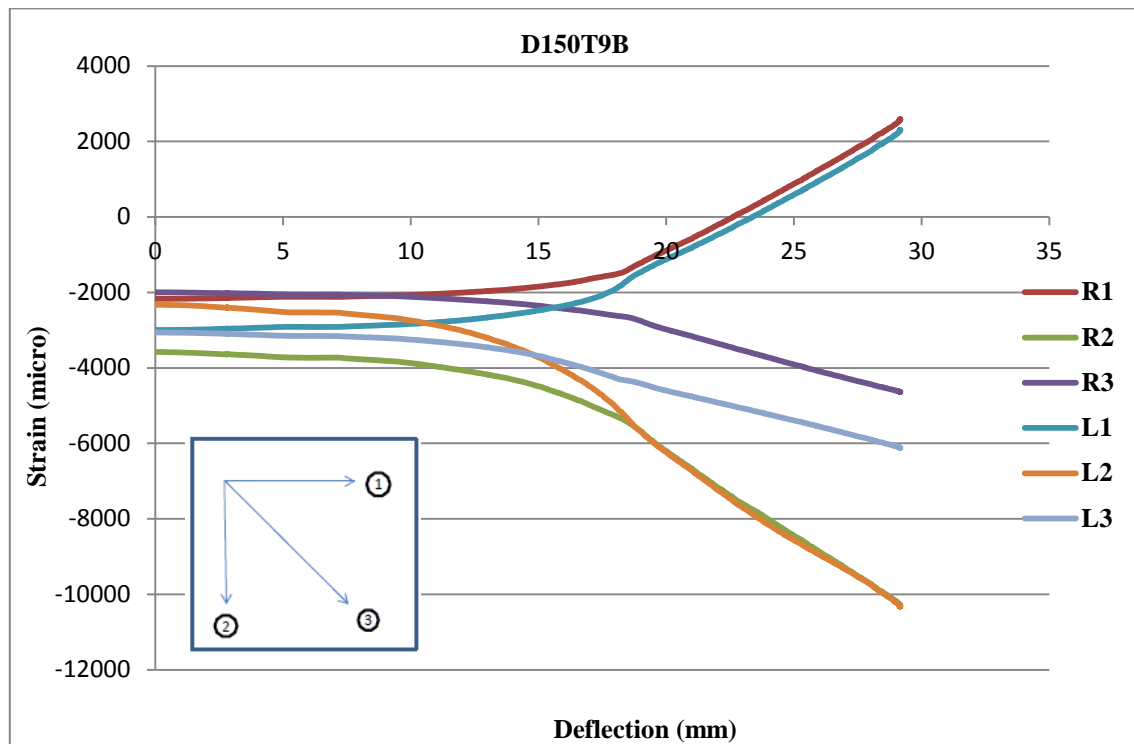


Figure 38: Strain-deflection behaviour of specimen D150T9B

4.3 Failure Mode and Equivalent Slenderness Ratio

Failure mode refers to how the columns failed under the compressive load; either buckling failure or compressive strength failure. Through this experiment, it was found that in all specimens except D150T8B, D150T9A and D150T9B, failure occurred in the form of buckling, and no friction of the FRP tubes was observed. At the same time, the ultimate load decreased with the slenderness ratio. As the specimens were composed of both FRP and concrete, the slenderness ratio is calculated as follows:

- The equivalent area of the cross section was estimated based on the elastic modulus of the FRP and concrete

$$A_{e,con} = A_c + \frac{E_{FRP}}{E_c} A_{FRP} \quad 4.2$$

Where,

$A_{e,con}$ - Equivalent area of concrete

A_c - Area of concrete

A_{FRP} - Area of FRP tube

E_c - Elastic modulus of concrete

E_{FRP} - Elastic modulus of FRP

- The slenderness ratio was calculated using the equation $\lambda = \frac{l_e}{r}$.

For a circular section, the radius of gyration is $r = D/4$ and for pin-supported columns the effective length is equal to the actual length. Therefore the slenderness ratio can be expressed by the following equation.

$$\lambda = 4 \frac{L}{D_e} \quad 4.3$$

Where

L - Length of the column

D_e - Equivalent diameter obtained from equation 4.2

The equivalent slenderness ratio for each specimens are summarised in Table 11. The equivalent slenderness ratios have a good correlation with the D/t value of the columns, as can be seen in the Figure 39.

Table 11: Variation of ultimate load with slenderness of the column

Specimen	Ultimate load (kN)	Total Area of column (mm²)	Equivalent Slenderness ratio (λ)	D/t
D100T3B	320	8 016	86.26	28.57
D100T3B	281	8 016	92.06	28.57
D100T8A	481	8 226	71.28	12.50
D100T8B	505	8 226	69.57	12.50
D100T9A	594	8 274	64.33	11.11
D100T9B	498	8 274	70.25	11.11
D150T3A	663	17 914	89.59	42.86
D150T3B	601	17 914	94.10	42.86
D150T8A	901	18 228	77.52	18.75
D150T8B	931	18 228	76.27	18.75
D150T9A	928	18 298	76.54	16.67
D150T9B	932	18 298	76.37	16.67

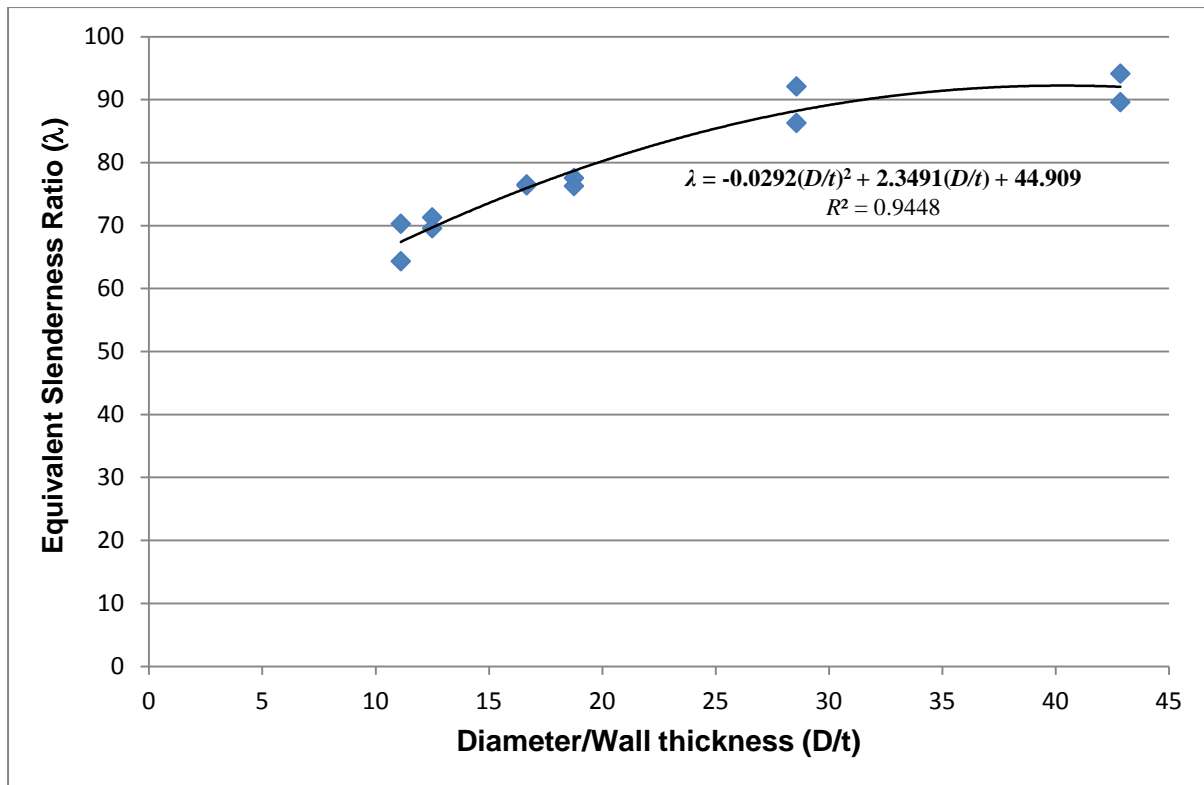


Figure 39: Variation of equivalent slenderness ratio with D/t ratio

4.4 General Observations

4.4.1 Bonding between FRP and Concrete

Even though FRP has increased in popularity for structural applications in recent years, the main issues with the FRP are

1. Low elastic modulus
2. Bonding with concrete.



Figure 40: De-bonding between FRP tube and concrete column

As shown in Figure 40, de-bonding was observed during the test. Unlike the bonding between steel and concrete, FRP did not attach to the concrete surface as one material. This meant that the two materials did not behave in the same way when load was applied.

4.4.2 Permanent Deformation in FRP pipes

The permanent deformation of the columns was recorded after the load was removed. The permanent deformation values are summarised in Table 12. From the table it can be seen the permanent deformation is high in the columns with high slenderness ratios.

Table 12: Permanent deformation of the specimens

Column	Maximum Vertical Deflection (mm)	Permanent Deformation (mm)
D100T3B	34.17	22.29
D100T3B	30.53	11.83
D100T8A	28.62	6.95
D100T8B	32.31	18.62
D100T9A	36.23	15.54
D100T9B	33.78	14.20
D150T3A	39.34	12.00
D150T3B	43.83	18.73
D150T8A	55.63	18.33
D150T8B	34.65	12.00
D150T9A	35.55	2.00
D150T9B	29.17	11.30



Chapter 5

CONCLUSIONS

The chief objectives and history of this project are presented in the first and second chapters of this thesis. The details related to the experimental program that was undertaken to achieve the objectives are stated in subsequent chapters. In this chapter, the conclusions of this research study will be shown in order to provide effective ways to adjust FRP columns to practical uses.

5.1 Conclusions

5.1.1 Main Conclusion

From the experimental study, it is concluded the diameter-to-wall thickness (D/t) of the FRP influences the capacity of CFT with FRP tubes, particularly when buckling failure is significant. From the experimental study, the slenderness ratio of the combined column was estimated. The proposed equivalent slenderness ratio has a good correlation with the D/t ratio of the FRP tube.

5.1.2 Specific Conclusions

According to the results of this experimental program as explained in the previous chapter, the following conclusions were reached:

- Equivalent slenderness ratio increases as D/t ratio increases. That means the strength of FRP columns filled with concrete will increase as D/t ratio decreases.
- The capacity of the column decreased when the diameter of the tube decreased. As the height of the columns was kept constant at 1200 mm, it can be concluded that the strength of FRP columns filled with concrete decreases as L/D ratio increases
- The wall thickness of the FRP tube is a more important (sensitive) parameter than the diameter of the tube – as increasing the thickness from D100T3B to D100T8A the

strength increases from 36.8 MPa to 50.9 MPa while increasing the diameter from D100T3B to D150T3A changes the strength from 36.8 MPa to 34.5 MPa.

- As expected a low slenderness ratio of columns is associated with less likelihood of buckling failure.

5.2 Recommendation for Future Studies

Based on the range of studies described in the literature review and the results of this study, the following recommendations are presented for future studies in this area of '*the behaviour of concrete columns confined with FRP tubes*'.

- More studies similar to those that have already been conducted are needed in order to investigate different types of FRP materials and the properties of concrete.
- During the test, loading on the specimens needs to continue until they fracture as the experimental results of this program do not show a whole procedure of failure. Through this additional step a more accurate investigation of the behaviour of the specimens is expected.
- It is also suggested that a higher capacity load cell is required in order to extend the range of tests as some of specimens for this program could not be tested due to the load cell capacity that this would have required.
- Detailed finite element analysis would significantly enhance this research project.

REFERENCES

- ACI Committee 318 2008, 'Building Code Requirements for Structural Concrete and Commentary (Metric Version)', *Concrete International*, vol. 30, no. 8, pp. 88-88.
- ACI Committee 440 1996, State-of-the-Art Report on Fiber Reinforced Plastic (FRP) Reinforcement for Concrete Structures: 29-31
- ACMA 2004, Definition of FRP Composites, American Composites Manufacturers Association, http://www.mdacomposites.org/mda/frp_def.html
- Antonio, N & Nick, MB 1994, 'FRP jacketed concrete under uniaxial compression', *Construction and Building Materials*, vol. 9, pp. 115-124.
- Barczak, TM & Tadolini, SC 2005, 'Standing Support Alternatives in Western Longwalls', *2005 SME Annual Meeting, Feb 28-Mar 2 2005*, p. 10.
- Becque, J, Patnaik, AK & Rizkalla, SH 2003, 'Analytical models for concrete confined with FRP tubes', *Analytische Modelle für Zementsäulen, die mit FRP -Rohren (anstelle von Stahlrohren) umkleidet sind*, no. 1, p. 31.
- Bouchelaghem, H, Bezazi, A & Scarpa, F 2011, 'Strength of concrete columns externally wrapped with composites under compressive static loading', *Journal of Reinforced Plastics & Composites*, vol. 30, no. 19, pp. 1671-1688.
- Buyukozturk, O & Hearing, B 1998, 'Failure Behavior of Precracked Concrete Beams Retrofitted with FRP', *Journal of Composites for Construction*, vol. 2, no. 3, p. 138.
- Choi, KK & Xiao, Y 2010, 'Analytical Studies of Concrete-Filled Circular Steel Tubes under Axial Compression', *Journal of Structural Engineering*, vol. 136, no. 5, pp. 565-573.
- Dandapat, R, Deb, A & Bhattacharyya, SK 2011, 'Failure modes for FRP wrapped cylindrical concrete columns', *Journal of Reinforced Plastics & Composites*, vol. 30, no. 7, pp. 561-579.
- Gardner, N & Jacobson, E 1967, 'Structural behaviour of concrete-filled steel tubes', *Journal of the American Concrete Institute*, vol. 64, p. 9.
- Han, LH 2007, *Concrete-filled steel tubular structures* [in Chinese], 2nd edn, Science Press, Beijing, China.
- Hosotani, M, Kawashima, K & J, H 1996, 'Seismic retrofit of reinforced concrete bridge piers by carbon fiber sheets', *Proceedings of the 1st US-Japan Workshop on Seismic Retrofit of Bridges*, Technical Memorandum of PWRI, No. 3481.
- Hsuan-Teh, H, Chiung-Shiann, H, Ming-Hsien, W & Yih-Min, W 2003, 'Nonlinear Analysis of Axially Loaded Concrete-Filled Tube Columns with Confinement Effect', *Journal of Structural Engineering*, vol. 129, no. 10, p. 1322.
- Huang, CS, Yeh, YK, Liu, GY, Hu, HT, Tsai, KC, Weng, YT, Wang, SH & Wu, MH 2002, 'Axial Load Behavior of Stiffened Concrete-Filled Steel Columns', *Journal of Structural Engineering*, vol. 128, no. 9, p. 1222.

Liang, M, Wu, Z-M, Ueda, T, Zheng, J-J & Akogbe, R 2012, 'Experiment and modeling on axial behavior of carbon fiber reinforced polymer confined concrete cylinders with different sizes', *Journal of Reinforced Plastics & Composites*, vol. 31, no. 6, pp. 389-403.

Liang, QQ 2009, 'Performance-based analysis of concrete-filled steel tubular beam-columns, Part II: Verification and applications', *Journal of Constructional Steel Research*, vol. 65, no. 2, pp. 351-362.

Manojkumar, VC, Mattur, CN & Kulkarni, SM 2010, 'Axial strength of circular concrete-filled steel tube columns – DOE approach', *Journal of Constructional Steel Research*, vol. 66, pp. 1248-1260.

Mirmiran, A & Shahawy, M 1997, 'Behavior of concrete columns confined by fiber composites', *Journal of Structural Engineering*, vol. 123, no. 5, p. 583.

Mirmiran, A, Shahawy, M, Samaan, M, Echary, HE, Mastrapa, JC & Pico, O 1998, 'Effect of Column Parameters on FRP-Confined Concrete', *Journal of Composites for Construction*, vol. 2, no. 4, p. 175.

Mohamed, HM & Masmoudi, R 2010, 'Axial Load Capacity of Concrete-Filled FRP Tube Columns: Experimental versus Theoretical Predictions', *Journal of Composites for Construction*, vol. 14, no. 2, pp. 231-243.

O'Shea, MD & Bridge, RQ 1998, 'Tests on Circular Thin-walled Steel Tubes Filled with Medium and High Strength Concrete', *Australian Civil Engineering Transactions*, vol. 40, p. 15.

Oral, B, Oguz, G & Erdem, K 2003, 'Progress on understanding debonding problems in reinforced concrete and steel members strengthened using FRP composites', *Construction and Building Materials*, vol. 18, pp. 9-19.

Richart, F, Brandtzaek, A & Brown, R 1928, *A study of the failure of concrete under combined compressive stresses*, University of Illinois at Urbana Champaign, College of Engineering. Engineering Experiment Station, Bulletin no. 185 v. 26, no. 12.

Rousakis, T & Karabinis, A 2012, 'Adequately FRP confined reinforced concrete columns under axial compressive monotonic or cyclic loading', *Materials & Structures*, vol. 45, no. 7, p. 957.

Samaan, M, Mirmiran, A & Shahawy, M 1998, 'Model of concrete confined by fiber composites', *Journal of Structural Engineering*, vol. 124, no. 9, p. 1025.

Schneider, SP 1998, 'Axially loaded concrete-filled steel tubes', *Journal of Structural Engineering*, vol. 124, no. 10, p. 1125.

Sundarraja, MC & Prabhu, GG 2011, 'Investigation on strengthening of CFST members under compression using CFRP composites', *Journal of Reinforced Plastics & Composites*, vol. 30, no. 15, pp. 1251-1264.

Tomii, M, Yoshimura, K & Morishita, Y 1977, 'Experimental studies on concrete-filled steel stub columns under concentric loading', *International Colloquium on Stability of Structural Under Static and Dynamic Loads*, p. 24.

Xiao, Y & Wu, H 2000, 'Compressive behavior of concrete confined by carbon fiber composite jackets', *Journal of Materials in Civil Engineering*, vol. 12, no. 2, p. 139.

Yu-Feng, A, Lin-Hai, H & Xiao-Ling, Z 2012, 'Behaviour and design calculations on very slender thin-walled CFST columns', *Thin-Walled Structures*, vol. 53, pp. 161-175.

Appendix A

EXPERIMENTAL DATA

A.1 Material properites

A.1.1 Concrete Strength

Batch	Cylinder	Diameter (mm)	Weight (g)	Concrete Strength (MPa)	Number of Day
1	1_1	199.0	3616.2	26.93	86
1	1_2	200.0	3624.2	35.18	86
1	1_3	199.0	3623.8	30.39	86
2	2_1	201.0	3613.1	27.56	80
2	2_2	201.0	3616.4	29.25	80
2	2_3	201.0	3561.5	33.25	80

A.1.2 Strain Gauges

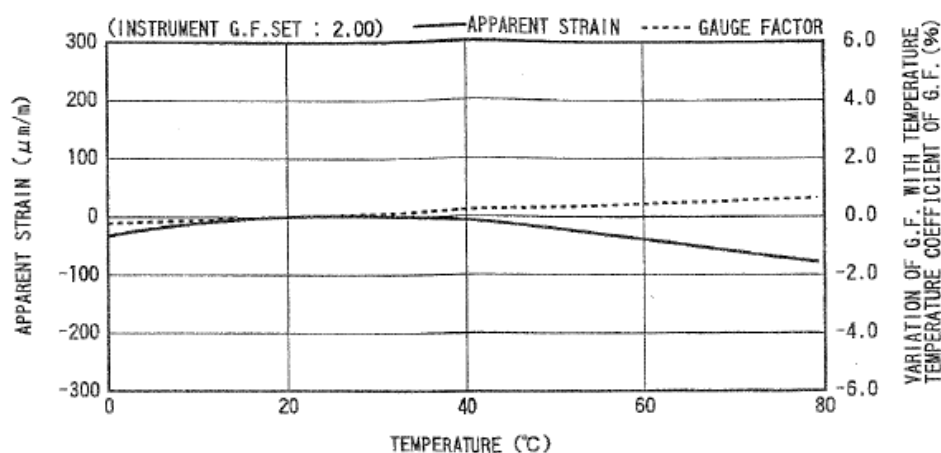
TML STRAIN GAUGE TEST DATA

GAUGE TYPE	: PFL-30-11	TESTED ON	: SS 400
LOT NO.	: A70361A	COEFFICIENT OF THERMAL EXPANSION	: 11.8 $\times 10^{-6}/^{\circ}\text{C}$
GAUGE FACTOR	: 2.11 $\pm 1\%$	TEMPERATURE COEFFICIENT OF G.F.	: $+0.11 \pm 0.05 \text{ } \%/^{\circ}\text{C}$
ADHESIVE	: P-2	DATA NO.	: D0053

THERMAL OUTPUT (ϵ_{app} : APPARENT STRAIN)

$$\epsilon_{\text{app}} = -3.26 \times 10^{-1} + 2.74 \times 10^{-2}T - 5.76 \times 10^{-2}T^2 + 8.05 \times 10^{-5}T^3 + 1.53 \times 10^{-6}T^4 \quad (\mu\text{m/m})$$

TOLERANCE : $\pm 0.85 [(\mu\text{m/m})/^{\circ}\text{C}]$, T : TEMPERATURE



ひずみゲージ取扱いの注意事項

- 上記の特性データは、リード線の取付けによる影響を含んでおりません。裏面記載のリード線の測定値への影響に従って補正してください。
- ゲージの使用温度は、接着剤の耐熱温度などにより変わります。
- 絶縁抵抗などの点検は、印加電圧を50V以下にしてください。
- ゲージリード線に無理な力を加えないでください。
- ゲージ裏面に接着剤を塗布して接着してください。
- ひずみゲージの裏面は脱脂洗浄してありますので、汚さないように取扱ってください。
- ゲージの包装を開封後は、乾燥した場所で保管してください。
- ご使用に際してご不明な点がございましたら、当社までお問い合わせください。

CAUTIONS ON HANDLING STRAIN GAUGES

- The above characteristic data do not include influence due to lead wires. Correct the data in accordance with the influence of lead wires on measured values described overleaf.
- The service temperature of strain gauge depends on the operating temperature of adhesive, etc.
- Check of insulation resistance, etc. should be made at a voltage of less than 50V.
- Do not apply an excessive force to the gauge leads.
- Apply an adhesive to the back of a strain gauge and stick the gauge to a specimen.
- As the back of strain gauge has been degreased and washed, do not contaminate it.
- After unpacking, store strain gauges in a dry place.
- If you have any questions on strain gauges or installation, contact TML or your local agent.

A.1.3 Load Cell

P02

Green wire positive.

TRANSDUCER DEVELOPMENT Co. Pty. Ltd.

P.O. Box 591, Archerfield, QLD. 4108. AUSTRALIA.
Phone. 07-3849-5143 Fax. 07-3849-4462
Intnl. ++61-7-3849-5143 ++61-7-3849-4462

LOAD CELL TEST CERTIFICATE.

Date : 08/06/1999

Model : HCC200

Ser. No. 6736

Date of Manufacture : 01/06/1999

Capacity :	200,000	Kilograms.
Excitation :	15	V. DC. Max.
Output Signal :	2.5126	mV / V.
Input Resistance :	700.0000	Ohms. +/- 10 %
Output Resistance :	700.0000	Ohms. +/- 1 %
Overload Capability :	150	% of FS. No Damage.
Ultimate :	400	% of FS. to Failure.
Temperature Range :	-10 to 90	Degrees C.
Effect on Zero :	0.0020	% / Degree C.
Effect on Span :	0.0020	% / Degree C.
Non Linearity :	0.1000	% of FS.
Hysteresis :	0.0200	% of FS.
Repeatability :	0.0200	% of FS.
Electrical Isolation :	5000	Meg Ohms.
Sealing Class :	IP 67	

TERMINATION.

MS3102E-14-S-6

Colour Coding :

Screen : Isolated.
Red : A (+) and
Green : F (+) and
Black : B (+) and

Black : D (-) Excitation.
White : E (-) Signal.
C (-) Sense.

CALIBRATION CHECK. (May Not Be Applicable)

A resistor connected across one bridge arm will produce an electrical signal proportional to an applied load.
The figures below were obtained during factory calibration.

Resistor Used :	0.00	Ohms.
Across Pins :	A-C	
Equivalent Load :		% of FS.

For IC, exc, calibration factor = 0.0000128 V/kN

BENEFITS AND FUNCTION

D633-D634

OPERATIONAL BENEFITS OF DIRECT DRIVE SERVO VALVES (DDV)

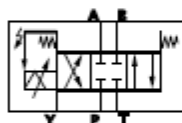
- Directly driven by a permanent magnet linear force motor with high force level
- No pilot oil flow required
- Pressure independent dynamic performance
- Low hysteresis and low threshold
- Low current consumption at and near hydraulic null
- Standardized spool position monitoring signal with low residual ripple
- Electric null adjust
- With loss of supply voltage or broken cable or emergency stop, the spool returns to its spring centered position without passing a load move position.

DIRECT DRIVE VALVE (DDV) OPERATION

The position control loop for the spool with position transducer and linear force motor is closed by the integrated electronics. An electric signal corresponding to the desired spool position is applied to the integrated electronics and produces a pulse width modulated (PWM) current to drive the linear force motor. An oscillator excites the spool position transducer (LVDT) producing an electric signal proportional to spool position.

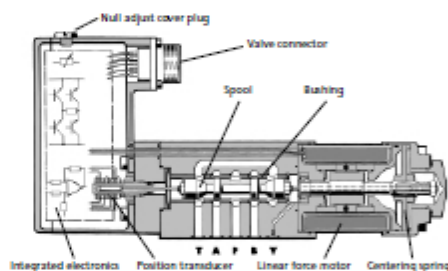
The demodulated spool position signal is compared with the command signal, and the resulting spool position error causes current in the force motor coil until the spool has moved to its commanded position and the spool position error is reduced to zero. The resulting spool position is thus proportional to the command signal.

D633 Series single stage Servo Control Valve



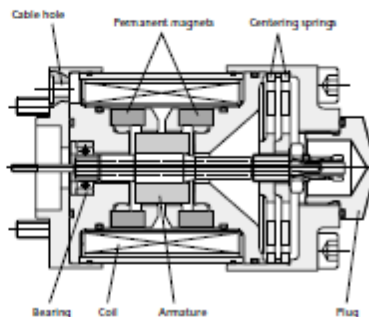
Hydraulic symbol:

Symbol shown with electric supply on and zero command signal.



PERMANENT MAGNET LINEAR FORCE MOTOR OPERATION

The linear force motor is a permanent magnet differential motor. The permanent magnets provide part of the required magnetic force. For the linear force motor the current needed is considerably lower than would be required for a comparable proportional solenoid. The linear force motor has a neutral mid-position from which it generates force and stroke in both directions. Force and stroke are proportional to current. High spring stiffness and resulting centering force plus external forces (i.e. flow forces, friction forces due to contamination) must be overcome during out-stroking. During backstroking to center position, the spring force adds to the motor force and provides additional spool driving force which makes the valve much less contamination sensitive. The linear force motor needs very low current in the spring centered position. Proportional solenoid systems require two solenoids with more cabling for the same function. Another solution uses a single solenoid, working against a spring. In case of current loss in the solenoid, the spring drives the spool to the end position by passing through a fully open position. This can lead to uncontrolled load movements.



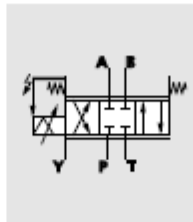
GENERAL TECHNICAL DATA, SYMBOLS

D633-D634

PERFORMANCE SPECIFICATIONS FOR STANDARD MODELS

Operating pressure range	
Ports P, A and B	up to 350 bar (5000 psi)
Port T	see data for individual series
Temperature range	
Ambient	-20 °C to +60 °C (-4°F to +140°F)
Fluid	-20 °C to +80 °C (-4°F to +170°F)
Seal material	NBR, FPM, others on request
Operating fluid	mineral oil based hydraulic fluid (DIN 51524, part 1 to 3), others on request
Viscosity	recommended 15 to 100 mm ² /s allowed 5 to 400 mm ² /s
System filtration	High pressure filter (without bypass, but with dirt alarm) mounted in the main flow and if possible directly upstream of the valve.
Class of cleanliness	The cleanliness of the hydraulic fluid particularly effects the performance (spool positioning, high resolution) and wear (metering edges, pressure gain, leakage) of the servo valve.
Recommended cleanliness class	
For normal operation	ISO 4406 < 15 / 12
For longer life (wear)	ISO 4406 < 14 / 11
Filter rating recommended	
For normal operation	$\beta_{10} \geq 75$ (10 μ m absolute)
For longer life (wear)	$\beta_{0.5} \geq 75$ (6 μ m absolute)
Installation options	any position, fixed or movable
Vibration	30 g, 3 axes
Degree of protection	EN60529: class IP 65 with mating connector mounted
Shipping plate	Delivered with an oil sealed shipping plate

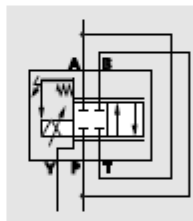
4-WAY FUNCTION



4-way version
spring centred

- Flow control (throttle valve) in port A and port B
- Port Y required if pressure $p_T > 50$ bar (715 psi) in port T
- for 3-way function close port A or port B of the manifold
- Spools with exact axis cut, 1,5 to 3 % or 10 % overlap available

2X2-WAY FUNCTION



2x2-way version
(Y-Port required)

- Flow control (throttle valve) in port A
- Port Y required
- Connect externally port P with port B, and port A with port T

GENERAL TECHNICAL DATA, ELECTRONICS

D633-D634

VALVE FLOW CALCULATIONS

The actual valve flow is dependent on the spool position and the pressure drop across the spool lands.

At 100% command signal (i.e. +10 VDC = 100% valve opening), the valve flow at rated pressure drop $\Delta p_N = 35$ bar per metering land is the rated flow Q_N . For other than rated pressure drop, the valve flow changes at constant command signal according to the square root function for sharp edged orifices.

$$Q = Q_N \sqrt{\frac{\Delta p}{\Delta p_N}}$$

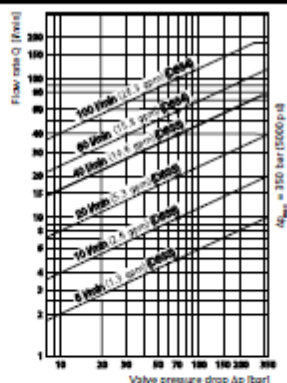
Q [l/min] = calculated flow

Q_N [l/min] = rated flow

Δp [bar] = actual valve pressure drop

Δp_N [bar] = rated valve pressure drop

The real valve flow Q calculated in this way should result in an average flow velocity in ports P, A, B or T of less than 30 m/s.



GENERAL REQUIREMENTS FOR VALVE ELECTRONICS

- Supply 24 VDC, min. 19 VDC, max. 32 VDC
- Current consumption I_{max}
 - for D633 1.2 A
 - for D634 2.2 A
- External fuse per valve
 - for D633 1.6 A (slow)
 - for D634 2.5 A (slow)
- All signal lines, also those of external transducers, shielded.
- Shielding connected radially to \perp (0 V), power supply side, and connected to the mating connector housing (EMC).
- EMC: Meets the requirements of emission: EN55011:1998+A1:1999 (limit class B) and immunity: EN61000-6-2:1999
- Minimum cross-section of all leads $\geq 0.75 \text{ mm}^2$ (0.001 in²). Consider voltage losses between cabinet and valve.
- Note: When making electric connections to the valve (shield, protective earth), appropriate measures must be taken to ensure that locally different earth potentials do not result in excessive ground currents. See also Moog Application Note TN 353.

VALVE ELECTRONICS WITH 24 VOLT SUPPLY VOLTAGE AND 6+PE POLE CONNECTOR

Command signal 0 to ± 10 mA

floating, Valves with current command input

The spool stroke of the valve is proportional to $I_0 - I_1$.

100 % valve opening P \rightarrow A and B \rightarrow T is achieved at $I_0 = +10$ mA. At 0 mA command the spool is in centered position. The input pins D and E are inverting. Either pin D or E is used according to the required operating direction. The other pin is connected to signal ground at cabinet side.

Command signal 0 to ± 10 V

Valves with voltage command input

The spool stroke of the valve is proportional to $(U_{D1} - U_{D2})$.

100% valve opening P \rightarrow A and B \rightarrow T is achieved at $(U_{D1} - U_{D2}) = +10$ V.

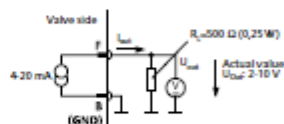
At 0 V command the spool is in centered position. The input stage is a differential amplifier. If only one command signal is available, pin D or E is connected to signal ground at cabinet side according to the required operating direction.

Actual value 4 to 20 mA

The actual spool position value can be measured at pin F (see diagram below). This signal can be used for monitoring and fault detection purposes.

The spool stroke range corresponds to 4 to 20 mA.

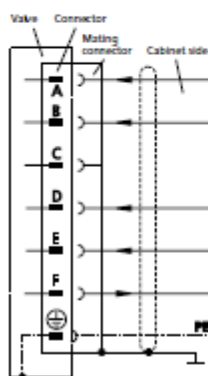
The centered position is at 12 mA. 20 mA corresponds to 100% valve opening P \rightarrow A and B \rightarrow T. The position signal output 4 to 20 mA allows detecting a cable break when $I_1 = 0$ mA.

Circuit diagram for measurement of actual value I_1 (position of spool) for valves with 6+PE pole connector

For failure detection purposes, it is advised to connect pin F of the mating connector and route this signal to the control cabinet.

WIRING FOR VALVES WITH 6+PE CONNECTOR

to EN 175201 Part 804¹⁾ and mating connector (type R and S, metal shell) with leading protective earth connection (\downarrow). See also Application Note AM 426 E.



Function	Current Command	Voltage Command
Supply	24 VDC (19 to 32 VDC)	
Supply / Signal Ground	± (0 V)	
Not used		
Input rated command (differential)	Input command $I_0 = -I_1$: 0 to ± 10 mA Input command (mV) $U_{D1} = -U_{D2}$: 0 to ± 10 V $R_L = 200 \Omega$	$U_{D1} = 0$ to ± 10 V $R_L = 10 \text{ k}\Omega$
Output actual value spool position	Input voltage for U_{D1} and U_{D2} for both signal types is limited to min. -15 V and max. +24 V. I_{F1} : 4 to 20 mA. At 12 mA spool is in centered position. $R_L = 200$ to 500Ω	
Protective earth		

¹⁾ formerly DIN 4362

TECHNICAL DATA

D633

PERFORMANCE SPECIFICATIONS FOR STANDARD MODELS

Model ... Type		D633
Mounting pattern with or without leakage port Y ¹⁾		ISO 4401-03-03-0-94
Port diameter	mm (in)	7.9 (0.31)
Valve version ²⁾		Single stage, spool in bushing
Spool actuation		3-way, 4-way, 2x2-way directly, with permanent magnet linear force motor
Pilot supply		none
Mass	kg (lb)	2.5 (5.5)
Rated flow (±10%) at Δp _v = 35 bar (500 psi) per land	l/min (gpm)	5 / 10 / 20 / 40 (1.3 / 2.6 / 5.3 / 10.6)
Max. valve flow	l/min (gpm)	75 (19.8)
Operating pressure max.		
Ports P, A, B	bar (psi)	350 (5000)
Port T without Y	bar (psi)	50 (715)
Port T with Y	bar (psi)	350 (5000)
Port Y	bar (psi)	directly to tank
Response time for 0 to 100% stroke, typical	ms	≤ 12
Threshold ³⁾	%	< 0.1
Hysteresis ³⁾	%	< 0.2
Null shift ³⁾ with ΔT = 55 K	%	< 1.5
Null leakage flow ³⁾ max. (axis cut)	l/min (gpm)	0.15 / 0.3 / 0.6 / 1.2 (0.04 / 0.08 / 0.16 / 0.32)

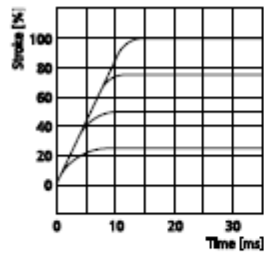
¹⁾ At operating pressure p_v = 140 bar (2000psi), fluid viscosity of 32 mm²/s (0.05 in²/s) and fluid temperature of 40 °C (104° F)

²⁾ See symbols page 4

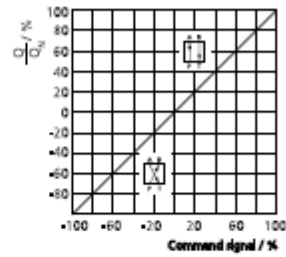
³⁾ Leakage port Y must be used
 ⇒ with 3- and 4-way function and p_T > 50 bar (715psi)
 ⇒ with 2x2-way function

CHARACTERISTIC CURVES (TYPICAL)

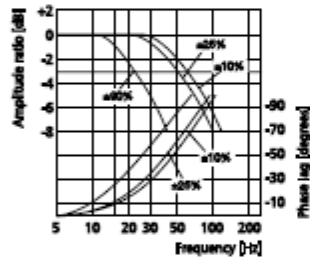
Step response



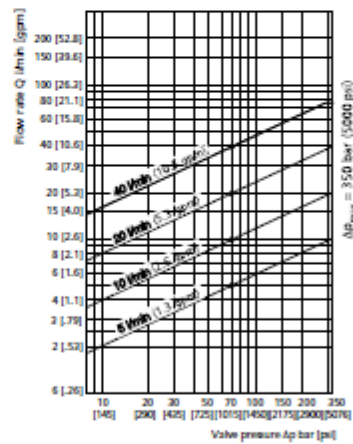
Flow signal characteristic curve



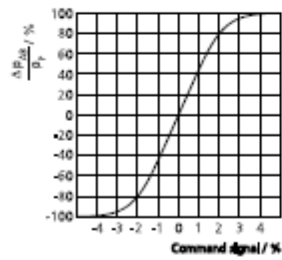
Frequency response



Valve flow diagram



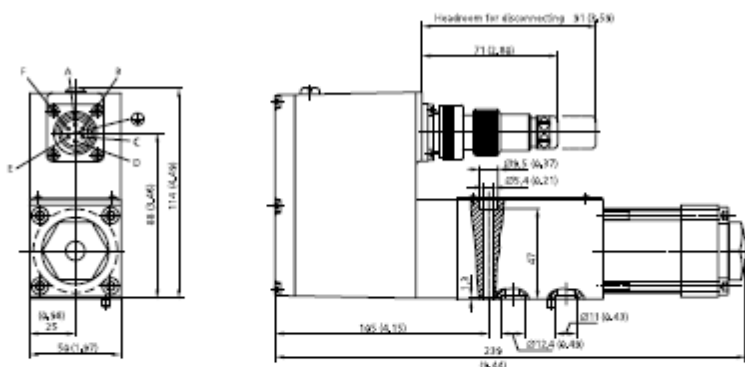
Pressure signal characteristic curve



TECHNICAL DATA

D633

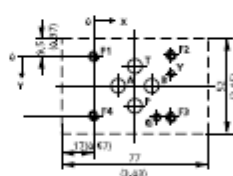
INSTALLATION DRAWING



Mounting pattern
ISO 4401-03-03-0-94, without X port


mm												
	P	A	B	T	X ¹⁾	Y	F ₁	F ₂	F ₃	F ₄	G	
x	27,5	27,5	27,5	27,5	0	0	M5	M5	M5	M5	4	
y	21,5	12,7	30,2	21,5	0	0	40,5	40,5	40,5	0	33	
	25,9	15,5	15,5	5,1	0	0	0,75	31,75	31	31,75		
inch												
	P	A	B	T	X ¹⁾	Y	F ₁	F ₂	F ₃	F ₄	G	
x	00,30	00,30	00,30	00,30	0	0	M5	M5	M5	M5	0,16	
y	0,85	0,50	1,19	0,85	0	0	1,60	1,60	1,60	0	1,30	
	1,02	0,61	0,61	0,20	0	0	0,03	1,25	1,22	1,25		

¹⁾ Port X must not be drilled, not sealed at valve base.



Mounting surface needs flat within 0,01 mm (0,0004 in) over a distance of 100 mm (3,94 in). Average surface finish value, Ra = 0,8 µm.

Spare parts and Accessories

O-rings (included in delivery)		NBR 90 Shore	FPM 90 Shore
for parts P,T,A,B	4 pieces ID 3,25 x Ø 1,8 (ID 0,36 x Ø 0,07)	45122-013	42082-013
for port Y	1 piece ID 7,65 x Ø 1,8 (ID 0,30 x Ø 0,07)	45122-012	42082-012
Mating connector, waterproof IP65 (not included in delivery)		for cable dia. min. Ø 10 mm (0,394 in), max. Ø 12 mm (0,472 in)	
6+PE-pole	837007-061	EN 175201 Part 804	
Flushing plates	for P,A,B,T,X,Y B46630-002		
Mounting manifolds	on request		
Mounting bolts (not included in delivery)	required torque	required	
M 5 x 55 DIN EN ISO 4762-10,9	AQ3665-050-055	8,5 Nm (75 inch pounds)	4 pieces

MOOG • D633/634 Series 9

TECHNICAL DATA

D634

PERFORMANCE SPECIFICATIONS FOR STANDARD MODELS

Model . . . Type		D634
Mounting pattern with or without leakage port Y ¹⁾		ISO 4401-05-05-0-94
Port diameter	mm (in)	11.5 (0.45)
Valve version ²⁾		Single stage, spool in bushing
Spool actuation		3-way, 4-way, 2x2-way directly, with permanent magnet linear force motor
Pilot supply		none
Mass	kg (lb)	6.3 (13.9)
Rated flow (±10%) at Δp _v = 35 (500 psi) bar per land	l/min (gpm)	60 / 100 (15.8 / 26.3)
Max. valve flow	l/min (gpm)	185 (48.8)
Operating pressure max.		
Ports P, A, B	bar (psi)	350 (5000)
Port T without Y	bar (psi)	50 (715)
Port T with Y	bar (psi)	350 (5000)
Port Y	bar (psi)	directly to tank
Response time for 0 to 100% stroke, typical	ms	≤ 20
Threshold ³⁾	%	< 0.1
Hysteresis ³⁾	%	< 0.2
Null shift ³⁾ with ΔT = 55 K	%	< 1.5
Null leakage flow ³⁾ max. (axis cut)	l/min (gpm)	1.2 / 2.0 (0.26 / 0.43)

¹⁾ At operating pressure p_v = 140 bar (2000 psi), fluid viscosity of 32 mm²/s (0.05 in²/s) and fluid temperature of 40 °C (104° F)

²⁾ See symbols page 4

³⁾ Leakage port Y must be used

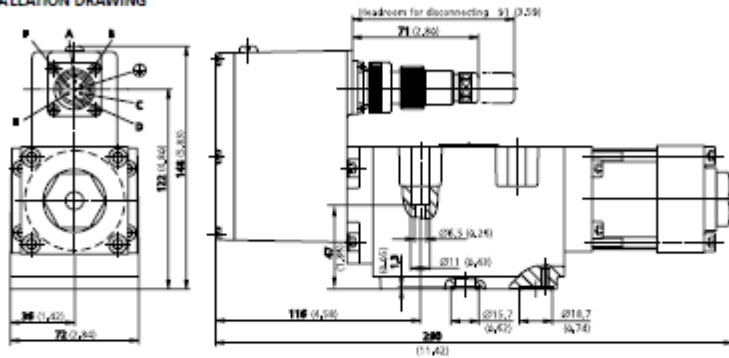
⇒ with 3- and 4-way function and p_T > 50 bar (715 psi)

⇒ with 2x2-way function

TECHNICAL DATA

D634

INSTALLATION DRAWING



Mounting pattern

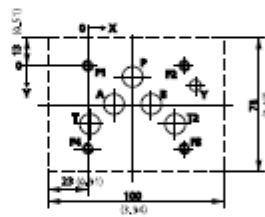
ISO 4401-05-05-0-94, without X port

mm

	P	A	B	T	T ₂	X ¹⁾	Y	F ₁	F ₂	F ₃	F ₄
	Ø11,2	Ø11,2	Ø11,2	Ø11,2	Ø11,2		Ø 6,3	M6	M6	M6	M6
x	27	16,7	37,3	3,2	50,8		62	0	54	54	0
y	6,3	21,4	21,4	32,5	32,5		11	0	0	46	46

inch


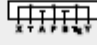

	P	A	B	T	T ₂	X ¹⁾	Y	F ₁	F ₂	F ₃	F ₄
	Ø0.44	Ø0.44	Ø0.44	Ø0.44	Ø0.44		Ø 0.25	M6	M6	M6	M6
x	1.06	0.66	1.47	0.13	2.00		2.44	0	2.13	2.13	0
y	0.25	0.84	0.84	1.28	1.28		0.43	0	0	1.81	1.81



¹⁾ Port X must not be drilled, not sealed at valve base.

Mounting surface needs flat within 0,01 mm (0.0004 in) over a distance of 100 mm (3.94 in). Average surface finish value, Ra = 0.8 µm.

Spare parts and Accessories

O-rings (included in delivery) for ports P, T, T ₂ , A, B for port Y	5 pieces ID 12,4 x Ø 1,8 (ID 5,49 x Ø 0,07) 1 piece ID 15,6 x Ø 1,8 (ID 6,11 x Ø 0,07)	NBR 90 Shore 45122-004 45122-011	FPM 30 Shore 42082-004 42082-011
Mating connector, waterproof PES (not included in delivery) 6-PE-pole	897007-001	EN 175201 Part 004	for cable dia min. Ø 10 mm (Ø.394 in), max. Ø 12 mm (Ø.472 in)
Flushing plates	for P, A, B, T, T ₂ , X, Y 867728-001		
Flushing plates	for P, A, B, T, T ₂ , X, Y 867728-002		
Flushing plates	for P, A, B, T, T ₂ , X, Y 867728-003		
Mounting manifolds	on request		
Mounting bolts (not included in delivery) M 6 x 60 DIN EN ISO 4762-16,9 A03665-060-060		required torque 13 Nm (115 inch pound)	required 4 pieces